Residual strength of blast damaged reinforced concrete columns

Xiaoli Bao, Bing Li*

School of Civil and Environmental Engineering, Nanyang Technological University, 50 Nanyang Ave, 639798, Singapore

Abstract

Columns are the key load-bearing elements in frame structures and exterior columns are probably the most vulnerable structural components to terrorist attacks. Column failure is normally the primary cause of progressive failure in frame structures. A high-fidelity physics-based computer program, LS-DYNA was utilized in this study to provide numerical simulations of the dynamic responses and residual axial strength of reinforced concrete columns subjected to short standoff blast conditions. The finite element (FE) model is discussed in detail and verified through correlated experimental studies. An extensive parametric study was carried out on a series of 12 columns to investigate the effects of transverse reinforcement ratio, axial load ratio, longitudinal reinforcement ratio, and column aspect ratio. These various parameters were incorporated into a proposed formula, capable of estimating the residual axial capacity ratio based on the mid-height displacement to height ratios.

Keywords:

Reinforced concrete column; Blast loadings; Numerical simulation; Residual axial capacity

1. Introduction:

Columns are the key load-bearing elements in frame structures. Exterior columns are probably the most vulnerable structural components to terrorist attacks. Column failure is normally the primary cause of progressive failure in frame structures. However, current knowledge in the evaluation of residual capacity of a blast damaged reinforced concrete column remains limited. A better understanding of residual capacity in columns would aid in the prediction of the overall performance of buildings, its resistance to progressive collapse and determining the stability of damaged buildings especially during search and rescue operations.

Single-degree-of-freedom (SDOF) analysis from blast-resistant design guidelines [1–3] provides engineers with simplified analytical methods to assess blast damage of RC columns. Although these simplified methods are quite useful, three-dimensional analysis, in contrast, provides a more in-depth understanding by incorporating all aspects of the response of concrete structures subjected to blast effects.

* Corresponding author: Tel.: +65 67905316

E-mail address: cbli@ntu.edu.sg (B. Li).

A study by Hayes *et al* [4] suggests that the proper application of current-practice seismic detailing for high-seismicity regions can reduce vulnerability to blasts and progressive collapse. One of the aims of this study is to quantify this improvement.

A three-dimensional nonlinear FE analysis utilizing the LS-DYNA software [5] is performed for the numerical simulations of this research. The FE model is validated through correlated experimental studies. The validated FE model was then analyzed under simulated blast loads and investigations were carried out on the dynamic responses and residual axial capacities of the columns. An extensive parametric study was carried out on a series of 12 columns to investigate the effect of the transverse reinforcement ratio, long-term axial load ratio, longitudinal reinforcement ratio, and column aspect ratio on the column responses.

2. Finite element model

The explicit nonlinear FEM program LS-DYNA [5] was utilized in this study because of its proven effectiveness in geometric modelling and impact analysis. The description of modelling includes blast loadings, the structural geometry, relevant material models, application of loads and analysis procedures.

2.1. Blast loadings

An exterior explosion to the building generates four types of loads as shown in Fig. 1: impact of primary fragments, impact of secondary fragments, overpressure, and reflected pressure. The study reported within this paper is restricted to the effects of overpressure and reflected pressure on the target from an explosion. As the overpressure wave strikes on the front face of a closed target, reflected pressure is instantly developed, and this is the most destructive aspect of blast loading on a structure. In this study, the explosion centre is assumed at the mid-height of a column, while the surface is assumed to be the reflected surface. The loading at different points on the front surface of the column for a given charge and standoff distance is computed by LS-DYNA [5] with the built-in CONWEP blast model, which relates the reflected overpressure to the scaled distance and also accounts for the angle of incidence of the blast wave [7]. Blast incidents in recent years showed that most of the terrorist attacks on public structures were explosions within short standoff distance (<10 m). Thus in this study, the standoff distance is assumed to be 5 m. Considering the limitation of the weight of the explosive which can be obtained in a particular region, a maximum weight of 1 ton equivalent TNT is presumed. Various charges weighing between 0 and 1 ton are used to obtain different levels of damage to the columns.

2.2. Structural geometry modelling

Fig. 2 shows the three-dimensional model of the column. Eight-node solid hexahedron elements are used to represent concrete. The reinforcing bars are modelled explicitly using two-node Hughes–Liu beam elements connected to the concrete mesh nodes. The nodes that link the concrete and reinforcement mesh are shared and these shared nodes are not able to slip. As a result, they form a perfect bond due to this assumption of complete compatibility of strains between concrete and steel. The restraint at the upper end of the column provided by secondary floor beams and slabs is modelled as a stiff block, while the bottom end restraint is modelled as a

fixed support. A rigid plate which is only allowed to move in the vertical direction is attached to the top end.

2.3. Material models

2.3.1. Concrete

The finite element code LS-DYNA, which is used in this research, contains several material models that can be used to represent concrete, namely, material type 5 (soil and crushable foam), material type 14 (soil and crushable foam failure), material type 16 (pseudo tensor), material type 25 (geological cap model), material type 72RW3 (concrete damage), material type 84 (winfrith concrete), and material type 96 (brittle damage). Material type 72RW3 (MAT_-CONCRETE_DAMAGE), was the third release of Karagozian and Case (K and C) concrete model. It is a plasticity-based model, using three shear failure surfaces and including damage and strain rate effects [8]. The model has a default parameter generation function based on the unconfined compressive strength of the concrete and provides a robust representation of complex concrete laboratory response [9]. In this model, the stress tensor is expressed as the sum of the hydrostatic stress tensor and the deviatoric stress tensor. The hydrostatic tensor changes the concrete volume and the deviatoric stress tensor controls the shape deformation.

For the hydrostatic stress tensor, the compaction model is a multi-linear approximation in internal energy. Pressure is defined by

$$p = C(\varepsilon_{\mathrm{v}}) + \gamma T(\varepsilon_{\mathrm{v}})E \tag{1}$$

where E is the internal energy per initial volume, γ is the ratio of specific heats. The volumetric strain, (ε_v); is given by the natural logarithm of the relative volume. As shown in Fig. 3 the model contains an elastic path from the hydrostatic tension cut-off to the point T of elastic limit. When tension stress is greater than the hydrostatic tension cut-off, tension failure occurs. When the volumetric strain exceeds the elastic limit, compaction occurs and the concrete turns into a granular kind of material. The bulk unloading modulus is a function of volumetric strain. Unloading occurs along the unloading bulk modulus to the pressure cut-off. Reloading always follows the unloading path to the point where unloading began, and continues on the loading path.

A three-curve model is used to analyze the deviatoric stress tensor, as shown in Fig. 4, where the upper curve represents the maximum strength curve, the middle curve is the initial yield strength curve and the lower curve is the failed material residual strength curve.

In order to consider the fact that under higher loading rates concrete exhibited increased strength, a dynamic increase factor (DIF), the ratio of the dynamic to static strength, is employed in this analysis. The expressions proposed by Malvar and Crawford [10,11] are utilized. The DIF for the concrete compressive strength is given as:

$$\mathrm{DIF} = \begin{cases} \left(\dot{\varepsilon}/\dot{\varepsilon}_{\mathrm{S}}\right)^{1.026\alpha_{\mathrm{s}}} & \dot{\varepsilon} \le 30\ \mathrm{s}^{-1} \\ \gamma_{\mathrm{S}}\left(\dot{\varepsilon}/\dot{\varepsilon}_{\mathrm{S}}\right)^{1/3} & \dot{\varepsilon} > 30\ \mathrm{s}^{-1} \end{cases} \tag{2}$$

where $\dot{\varepsilon}$ is the strain rate in the range of 30×10^{-6} to 300s^{-1}; $\dot{\varepsilon} = 30 \times 10^{-6} s^{-1}$(static strain rate); $\log \gamma_s = 6.156\alpha_s - 2; \alpha_s = 1/(5 + 9f_c/f_{co}), f_{co} = 10MPa$; f_c is the static compressive strength of concrete. A plot of the formulae employed in this study for the DIF of concrete in compression is shown in Fig. 5(a).

The DIF for concrete in tension is given by:

$$\text{DIF} = \begin{cases} \left(\dot{\varepsilon}/\dot{\varepsilon}_s\right)^{\delta} & \dot{\varepsilon} \leq 1.0\ \text{s}^{-1} \\ \beta\left(\dot{\varepsilon}/\dot{\varepsilon}_s\right)^{1/3} & \dot{\varepsilon} > 1.0\ \text{s}^{-1} \end{cases} \tag{3}$$

where $\dot{\varepsilon}$ is the strain rate in the range of 10^{-6} to 160s^{-1}; $\dot{\varepsilon}_s = 10^{-6} s^{-1}$(static strain rate);$\log \beta = 6\delta - 2; \delta = 1/(1 + 8f_c/f_{co}), f_{co} = 10MPa$; f_c is the static compressive strength of concrete. A plot of the formulae employed in this study for the DIF of concrete in compression is shown in Fig. 5(b).

Based on Fig. 5(a) and (b), it can be seen that the tensile response is more sensitive to strain rate than compressive response. Therefore, different rate enhancements are included in "tension and compression" in the concrete material model employed in this study.

In the numerical model, the strain rate effect is incorporated as follows. At any given pressure, the failure surfaces are expanded by a rate enhancement factor which depends on the effective deviatoric strain rate, as shown in Fig. 6. Let r_f be the strain rate enhancement factor and p the pressure; an "unenhanced"pressure p/r_f is first obtained, then the unenhanced strength $\Delta\sigma(p/r_f)$ is calculated for the specified failure surface. Finally, the enhanced strength is given by:

$$\Delta\sigma_e = r_f \Delta\sigma(p/r_f) \tag{4}$$

Strength is equally enhanced along any radial stress path, including uniaxial, biaxial and triaxial tension, and uniaxial and biaxial compression. The effective strain rate versus deviatoric strength enhancement is given by a LS-DYNA define curve keyword.

2.3.2. Reinforcement

Steel is modelled as a strain rate sensitive uniaxial elasto-plastic material to account for its strain rate sensitivity and stress–strain history dependence. The stress–strain curve is assumed to be bilinear, representing an elasto-plastic behaviour with linear isotropic hardening. For the strain rate sensitivity, the expressions proposed by Malvar and Crawford [10] are utilized. A plot of the proposed formulae is shown in Fig. 7.

The yield stress of reinforcement is represented by:

$$\text{DIF} = \left(\dot{\varepsilon}/10^{-4}\right)^{\alpha} \tag{5}$$

where $\alpha = \alpha_{fy}, \alpha_{fy} = 0.074 - 0.04 f_y/414$ and f_y is the static yield strength of reinforcement in MPa.

The ultimate stress of reinforcement is represented by:

$$\text{DIF} = \left(\dot{\varepsilon}/10^{-4}\right)^{\alpha} \quad (6)$$

where $\alpha = \alpha_{fu}, \alpha_{fu} = 0.019 - 0.009 f_u/414$ and f_u is the static ultimate strength of reinforcement in MPa.

2.4. Application of loads and analysis procedure

The behaviour of columns subjected to blast conditions will be influenced by the fact that in most cases, the columns would have already been subjected to their respective service prior to being exposed to blast effects. Therefore, in the first loading stage, gravity load is applied via slow ramps to the column, while in the second loading stage, blast and gravity loads are applied simultaneously. The gravity load includes both the dead and service loads acting on the column. The gravity loads are assumed to be in the range of $0.1— 0.4 f_c' A_g$ to investigate the effects of gravity load on the dynamic response and residual axial capacity of reinforced concrete columns under short standoff blast conditions. Eventually, in the post-blast loading stage, axial load is increased until the column is crushed, as shown in Fig. 8.

3. Verification of finite element model

Verification of the finite element models as outlined in the above procedure is carried out by performing the analysis of several correlated studies.

3.1. Dynamic testing on concentrically loaded reinforced concrete columns confined by square hoops

The transverse reinforcement is modelled using beam elements to take into account the confinement effect. In addition, the concrete material model has one parameter (b_1) that governs softening in compression. The axial load–strain curve of a small reinforced concrete column for a uniaxial compression test conducted by Mander *et al* was reproduced [12] for model calibration.

During the experiment, the column was loaded concentrically in a DARTEC 10 MN servohydraulically controlled testing machine. Because of the high oil-pumping capacity, a high axial strain rate could be achieved. For the selected specimen, the strain rate was $\varepsilon_c = 0.0167/s$. The axial strain was recorded over the central 400 mm gauge length of column using four linear potentiometers. The axial strain plotted is defined as the average strain occurring in those gauge lengths within the crushing region rather than the average strain of all gauge lengths. Therefore, the critical axial strain at the central portion of the column from the numerical analysis is used to match the experimental data. The experimental and analytical results are plot in Fig. 9. Agreement is close with the predicted peak axial load exceeding the experimental results by around 8%.

3.2. Reinforced concrete columns subjected to simulated blast loading

The first explosive loading laboratory testing program at the University of California, San Diego utilizes a hydraulic-based blast simulator to simulate explosive events without using explosive materials [13]. Several tests have been performed to investigate the dynamic response of the reinforced concrete columns when subjected to impulsive loads.

The dynamic responses of the test specimens subjected to impulse loads of 0.77 psi-s, 1.76 psi-s, 1.9 psi-s and 2.3 psi-s were analyzed using the proposed finite element models. Three cases of positive duration representative of the typical energy dissipation time of a close-in explosion, 3 ms, 4 ms, and 5 ms, and their respective peak pressure were utilized in the analysis, as the detailed peak pressure and duration for the corresponding impulse loads were not given.

Fig. 10 shows the comparisons of residual deformations of numerical, laboratory and field test results. These comparisons generally show a good agreement. The comparisons show that the numerical result is much higher than the laboratory test result when subjected to an impulse load of 1.76 psi-s. While for the other cases, the comparisons generally show a good agreement. Considering that only limited data are available and the unstable character of blast test results, these comparisons are considered to be reasonably in good agreement. Good correlations of failure mechanisms are also observed, as shown in Fig. 11. From both field test and blast simulator test results, it is apparent that the column failed primarily in diagonal shear near the top and bottom ends, with the central portion remaining relatively intact. The predicted damage on the column by the FE model is shown by plotting fringes of effective strain which is used for measuring the overall deformation at one point. These effective strain contours reveal the strain localization where failure propagates. It shows that the failure is localized near the column top and bottom ends due to diagonal shear failure, which is consistent with field and laboratory test results.

4. Numerical simulation study

4.1. Numerical simulation matrix

Using the finite element models discussed above, numerical simulations were performed to evaluate the dynamic response in blast situations, and to further estimate the residual axial capacity of the damaged columns. An extensive parametric study was carried out with the following cases considered for each parameter: transverse reinforcement ratio $\rho_v = 0.12\%$ and 0.46%; longitudinal reinforcement $\rho_g = 1.8\%$ and 3.2%; column aspect ratio $L/b = 9.8, 8$ and 6; axial load ratio $P_L/f_c'A_g = 0.1, 0.2, 0.3$ and 0.4. The parametric study was carried out using a series of 12 columns, labelled as series A–L, as shown in Fig. 12. The series B, D, F, H, J, and L are seismically detailed columns for which the spacing of the transverse reinforcement is determined in accordance with the requirement in the ACI 318 code. Table 1 summarises the specimen characteristics of the simulation matrix.

4.2. Numerical results of reinforced concrete columns in the dynamic response stage

4.2.1. Effect of transverse reinforcement ratio

Blast loadings are many times greater than conventional loads. The desired ductile flexural behaviour can only be developed when the shear capacity exceeds flexural capacity. The ductility capacity of a column depends on the amount and distribution of transverse reinforcement within the plastic hinge region. The transverse reinforcement increases the shear capacity of the column, but more importantly, it provides confinement to the core concrete and lateral restraint against buckling of the longitudinal reinforcement. Such restraint is vital for reinforced concrete columns which have begun to crack and have lost the majority of their tensile and flexural capacity but still need to bear compressive force until ductile failure of the longitudinal reinforcement occurs. Therefore,

transverse reinforcement is expected to have a significant influence on the failure mode of the columns under blast loading and their respective blast resistance. Fig. 13 shows the effect of the transverse reinforcement ratio on the displacement response of the columns. In these figures, the horizontal axis represents the magnitude of the impulse, which is obtained from the CONWEP software; the vertical axial y_r/L represents the displacement to height ratio, where y_r is the residual lateral displacement at mid-height and L is the clear height of the column. The dotted lines denote the numerical results, and the solid lines represent the fitted trend lines. Series A and C columns are conventional columns which are mainly designed for gravity loads and are weak in their shear capacity. Series B and D are seismically detailed columns. It can be seen that under the same impulsive loads, the shear-critical columns have a much larger deflection than the seismically detailed columns. This is consistent with the predication that implementation of seismic detailing can significantly reduce the degree of direct damage due to blast loads and consequently improve the blast resistance of the columns. The improvement becomes more remarkable in cases with severe impulsive loads.

4.2.2. Effect of axial load

Before the occurrence of a blast incident, the gravity load is already imposed on the column. This will influence the behaviour of the column under blast conditions. Fig. 14 illustrates the effect of axial load on the displacement response of the columns with a high transverse reinforcement ratio. As the figures demonstrate, when the impulsive loading and corresponding deformation are small, the mid-height displacement of the column with larger axial loads is slightly smaller. This is due to the fact that with an increase in the applied axial load on columns, it would result in an increase in its moment capacity and its nominal shear strength. However, the decrease in mid-height displacement would only occur before the impulse and its corresponding displacement reach a critical value. Once this critical value is exceeded, the mid-height displacement would increase greatly with increasing axial load. This is expected for columns with flexural behaviour. When columns experience large deflection and plastic hinges formation occurs at mid-span and fixed ends, axial loads will amplify the lateral deflection and internal moment due to the $P-\Delta$ effect. As the deflection increases, the column will transit from a gradual stiffness and strength degradation to a rapid loss of strength due to the buckling of the longitudinal reinforcement. This explains the change in the slope of the curve from gentle to steep as the axial loads increase.

Fig. 15 illustrates the effect of the axial load on the displacement response of the columns with a low transverse reinforcement ratio. When impulsive loading and the corresponding deformation are small, the mid-height displacement of the column with larger axial loads is slightly smaller, as shown in the figure. Columns with higher axial loads collapsed when the impulse loading and corresponding deformation were small due to the brittle behaviour of shear-critical columns. Thus, there is less data for columns with higher axial loads shown in the figure. It is believed that axial load failure occurred immediately after the shear failure; while for the columns having lower axial loads, the collapse only occurred when the impulsive loading and corresponding deformation are relatively large, although shear failure had occurred at a smaller displacement ratio. This may be due to the following factor: the longitudinal reinforcement will support a portion of the axial load up to a maximum load defined by either the buckling (bulking length equal to the spacing of ties) or the plastic capacity of the reinforcement bars; when the axial loads were less than this capacity, the axial load collapse didn't occur until the ductile failure of the reinforcement. Therefore, the columns under low axial loads tend to have a more ductile response than those under high axial loads.

Similar findings have been reported for both reinforced concrete columns and shear walls during seismic investigations [14].

4.2.3. Effect of longitudinal reinforcement ratio

As the longitudinal reinforcement ratio increases, both the ultimate moment capacity and axial capacity increase. As a result, an increase in longitudinal reinforcement ratio would improve the blast resistance of the column with flexural behaviour. Fig. 16(a) illustrates the effect of the longitudinal reinforcement ratio on the displacement response of the columns with a high transverse reinforcement ratio. The results show that the mid-height displacement decreases with increasing longitudinal reinforcement ratio as expected. However, an increase in longitudinal reinforcement may not always improve the blast resistance. When the flexural capacity of the column exceeds its shear capacity, it may lead to a shift from a ductile flexural failure to a brittle shear failure mode. In such cases, the mid-height displacement will increase with increasing longitudinal reinforcement ratio. Fig. 16(b) shows the effect of longitudinal reinforcement for columns with a low transverse reinforcement ratio. In this figure, series A columns are critical in shear due to inadequate transverse reinforcement, and series C columns are critical in flexure due to the fact that they have lesser flexural capacity than shear capacity because of the low longitudinal reinforcement ratio. As the figures demonstrate, when the impulsive loading and corresponding deformation are small, the mid-height displacement of series A column is larger than that of the series C column. This is consistent with the prediction above. However, when the impulsive loading and corresponding deformation are large, the mid-height displacement of series C column is larger than that of series A column. This is believed to result from the $P-\Delta$ effect for flexural columns when the deflection is large. Flexural failure is preferred than shear failure because an extended plastic response is provided prior to the collapse of column. However, it is noteworthy that the deformation in flexure beyond a certain limit will jeopardize the ability of the column to carry vertical loads due to the $P-\Delta$ effect. Therefore, to improve the blast resistance and assure a ductile response, sections need to be designed so that the flexural capacity is less than the capacity of non-ductile failure mechanism and the deflection must be controlled to prevent column instability due to the $P-\Delta$ effect.

4.2.4. Effect of column aspect ratio

In this study, the cross section is kept constant for all the column specimens. A decrease in column aspect ratio means a decrease of overall height. As a result, when subjected to the same intensity of blast loads, the moment and shear demand will decrease with decreasing column aspect ratio. The effect of aspect ratio on the displacement response is shown in Fig. 17. It is observed that under the same impulsive loading the displacement to height ratio decreases with a reduced aspect ratio as expected. Based on the figures, the results are similar for both shear-critical and flexural columns.

4.3. Numerical results of residual axial capacity of the blast damaged reinforced concrete

In the post-blast analysis stage, the axial load is gradually increased by applying a rigid plate attached to the top end of the column using the displacement mode to capture both the residual axial capacity and the softening portion of the loading curve. One typical curve is shown in Fig. 18. It is noted that in the blast loading stage, due to the inertia effect, the axial load supported by the column is not constant but fluctuates along the deformation of the column. The sudden increase of the axial force at a displacement of 75 mm could be due to the steel reinforcing bars reaching their strain

hardening stage. The increase in the strength of the steel reinforcement at this point in time would result in an increase in the columns axial load carrying capacity. The ultimate state of reinforced concrete columns has often been defined by some researchers [15] as a state of vanishing axial capacity to sustain the dead and live loads (long-term load), which is indicated as the point of axial failure (Fig. 19).

4.3.1. Post-blast damage evaluation

In this study, the residual axial capacity level of a blast damaged column was evaluated by the ratio of residual axial strength, which was defined by the following equation:

$$v = (P_{\mathrm{r}} - P_{\mathrm{L}})/(P_{\max} - P_{\mathrm{L}}) \tag{7}$$

where P_{max} is the axial capacity of the undamaged columns, P_r is the residual axial capacity of the damaged columns and P_L is the long-term axial load.

When the column is undamaged, $P_r = P_{max}$, the value of v is 1; when the column has lost the ability to sustain the long-term axial load, $P_r = P_L$, the value of v just reaches zero, referring as the ultimate state of the column. As for the performance indicator, the previously defined displacement to height ratio (y_r/L) is used.

4.3.2. Effect of axial load ratio

Fig. 19 shows the effect of axial load ratio on the residual axial capacity of the columns at various degrees of deformation level. The results show that at the same mid-height displacement ratio, the ratio of residual axial capacity is smaller in the case of larger axial loads. As illustrated by the figure, for columns with lower axial loads, the axial load failure tends to occur at a relatively large displacement ratio; for columns with a larger axial load, axial load failure tends to occur at a smaller displacement ratio. This indicates that the displacement ratio at axial load failure is inversely related to the magnitude of axial load. It is also noted that for columns with a low transverse reinforcement ratio, the effect of axial load is more critical. This is believed to be due to the significance of confinement during axial compression.

Based on the observation, a new term $(y_r/L) \times (P_L/f_c'A_g)$was introduced. Fig. 20 plots the relation between v and $(y_r/L) \times (P_L/f_c'A_g)$ for the columns. It can be seen that this new term is capable of reflecting the influence of the axial load ratio on the ratio of residual axial capacity. It also highlights the effects of other parameters and enables them to be studied based on the comparison of v versus $(y_r/L) \times (P_L/f_c'A_g)$curves.

4.3.3. Effect of longitudinal reinforcement ratio

It is usually assumed that longitudinal reinforcement will support a portion of the axial load up to a maximum load defined by either the buckling or the plastic capacity of the reinforcing bars. In most cases the column collapse is related to the increase of axial load carried by the longitudinal reinforcing bars and their deterioration of compressive strength. Fig. 21 shows the effect of the longitudinal reinforcement ratio on the residual axial capacity ratio of the columns. The results indicate that the ratio of residual axial capacity is generally larger when the longitudinal reinforcement ratio increases.

4.3.4. Effect of transverse reinforcement ratio

Fig. 22 shows the effect of the transverse reinforcement ratio on the residual axial capacity of the columns at various degrees of deformation level. The results show that the ratio of residual axial capacity of columns with a low transverse reinforcement ratio is significantly less than that of the column with a high transverse reinforcement ratio. From these figures, it is observed that under similar axial loading conditions, axial load failure tends to occur at a relatively large displacement ratio for columns with high transverse reinforcement ratio. In contrast, columns with a low transverse reinforcement ratio will tend to fail under axial loads at a smaller displacement ratio. This suggests that the displacement ratio at axial load failure is directly related to the transverse reinforcement ratio.

4.3.5. Effect of column aspect ratio

Fig. 23 illustrates the effect of the column aspect ratio on the residual axial strength ratio of the columns. The results show that at a high transverse reinforcement ratio, the residual axial capacity ratio increases with the reduction in aspect ratio. For columns with a low transverse reinforcement ratio, this effect is not very clear due to the scatter in the results.

4.4. Proposed formulae for determining the residual axial capacity ratio of blast damaged reinforced concrete columns

The parametric study carried out revealed the significance of the parameters that affect the residual axial strength of the blast damaged reinforced concrete column. A formula was derived through multivariable regression analysis in terms of various parameters to predict the residual axial capacity ratio based on the mid-height displacement to height ratio by fitting the parametric study results and is as follows:

$$v = \left[73.65\rho_v + 8.465\rho_g - 0.020879(L/b) + 0.104\right] e^{\left[89284.22\rho_v - 1308.64221\rho_g - 9.684203(L/b) - 382.12\right](y_t/L)(P_L/f'_cA_g)} \quad (8)$$

A few examples presenting the comparison of the proposed equation with the analytical results are shown in Fig. 24. The solid line in each plot denotes the proposed equation, while the dotted line represents the numerical analysis results. It is observed that for most parts, the proposed curves are close to the analytical results.

5. Summary and conclusions

Based on the results of the parametric study, the following main conclusions can be drawn.

- The numerical results show that the use of seismic detailing techniques can significantly reduce the degree of direct blast-induced damage and subsequent collapse of the reinforced concrete columns.
- Comparisons of the deterioration of the axial strength under different axial load ratios indicate that the ratio of residual axial strength is smaller under larger long-term axial load. The effect of axial load ratio is more critical in the case of columns with a low transverse reinforcement ratio.

- The results indicate that the ratio of residual axial capacity generally increases with an increase in the longitudinal reinforcement ratio.
- The numerical results indicate that the residual axial capacity ratio increases with a reduction in the aspect ratio for columns with a high transverse reinforcement ratio.
- A formula was derived by fitting the parametric study results, in terms of various parameters to predict the residual axial capacity ratio based on the mid-height displacement to height ratio. The comparison of the proposed equation with the analytical results shows that the proposed curve well represents the tendency with the variation of the parameters. Future experimental investigation of residual axial strength of the blast damaged reinforced concrete columns is needed to further supplement the limited data set used to develop the proposed equation.

Acknowledgements

This research was supported by a research grant provided by the Defense Science and Technology Agency (DSTA), Singapore, under the Protective Technology Research Center, Nanyang Technological University, Singapore. Any opinions, findings and conclusions expressed in this paper are those of the writers and do not necessarily reflect the view of DSTA, Singapore.

References

[1] TM 5-855-1 Fundamentals of protective design for conventional weapons. Washington D.C.: United States Department of the Army; 1986.

[2] TM5-1300 Structures to resist the effects of accidental explosions. In: Reinforced concrete design, vol. IV. Washington D.C.: United States Department of the Army; 1990.

[3] Hai-Cheng Rong, Bing Li. Deformation-controlled design of RC flexural members subjected to blast loadings. ASCE. Journal of Structural Engineering Oct 2008;134(10):1598–610.

[4] Hayes JR, Woodson SC, Pekelnicky RG, Poland CD, Corley WG, Sozen M. Can strengthening for earthquake improve blast and progressive collapse resistance? ASCE. Journal of Structural Engineering 2005;131(8):1157–77.

[5] LS-DYNA keyword user's manual, version 971. Livermore (CA), USA: Livermore Software Technology Corporation; 2006.

[6] Naito CJ, Wheaton KP. Blast assessment of load-bearing reinforced concrete shear walls. ASCE. Practice Periodical on Structural Design and Construction 2006;11(2):112–21.

[7] Randers-Pehrson G, Bannister KA. Airblast loading model for DYNA2D and DYNA3D. Army Research Laboratory. Report ARL-TR-1310, publicly released with unlimited distribution; 1997.

[8] Malvar LJ, Crawford JE, Wesevich JW, Simons D. A plasticity concrete material model for DYNA3D. International Journal of Impact Engineering 1997; 19(9–10):847–73.

[9] Schwer L, Malvar LJ. Simplified concrete modeling with *MAT_CONCRETE_ DAMAGE_REL3. LS-DYNA Anwenderforum, H-I-49-60, Bamberg; 2005. Malvar LJ, Crawford JE. Dynamic increase factors for steel reinforcing bars. Twenty-eighth DDESB seminar, Orlando, FL; 1998.

[10] Malvar LJ, Crawford JE, Morrill KB. K and C concrete material model, release III – automated generation of material model input. Karagozian and Case structural engineers. Technical report 2000 TR-99-24.3.

[11] Mander JB, Priestly MJN, Park R. Observed stress–strain behaviour of confined concrete. ASCE. Journal of Structural Engineering 1988;114(8): 1827–57. Hegemier GA, Seible F, Rodriguez-Nikl T, Arnett K. Blast mitigation of critical infrastructure components and systems. Proceedings of the 2nd international congress, Naples, Italy; 2006.

[12] Erduran E, Yakut A. Drift based damage functions for reinforced concrete columns. Computers and Structures 2004;82:121–30.

[13] Tasai A. Residual axial capacity and restorability of reinforced concrete columns damaged due to earthquake. Technical report, Pacific Earthquake Engineering Research Centre (PEER), 1999/10: 191–202; 1999

List of Tables

List of Figures

Column type	Cross section	Column height	Aspect ratio	Long. steel	Transverse steel
A	355 × 355 mm (14 × 14 in)	3480 mm (137 in)	9.8	8T25 ($\rho_g = 3.2\%$)	T10–350 mm ($\rho_v = 0.12\%$)
B	355 × 355 mm (14 × 14 in)	3480 mm (137 in)	9.8	8T25 ($\rho_g = 3.2\%$)	T10–88 mm ($\rho_v = 0.46\%$)
C	355 × 355 mm (14 × 14 in)	3480 mm (137 in)	9.8	8T20 ($\rho_g = 1.8\%$)	T10–350 mm ($\rho_v = 0.12\%$)
D	355 × 355 mm (14 × 14 in)	3480 mm (137 in)	9.8	8T20 ($\rho_g = 1.8\%$)	T10–88 mm ($\rho_v = 0.46\%$)
E	355 × 355 mm (14 × 14 in)	2840 mm (112 in)	8	8T25 ($\rho_g = 3.2\%$)	T10–350 mm ($\rho_v = 0.12\%$)
F	355 × 355 mm (14 × 14 in)	2840 mm (112 in)	8	8T25 ($\rho_g = 3.2\%$)	T10–88 mm ($\rho_v = 0.46\%$)
G	355 × 355 mm (14 × 14 in)	2840 mm (112 in)	8	8T20 ($\rho_g = 1.8\%$)	T10–350 mm ($\rho_v = 0.12\%$)
H	355 × 355 mm (14 × 14 in)	2840 mm (112 in)	8	8T20 ($\rho_g = 1.8\%$)	T10–88 mm ($\rho_v = 0.46\%$)
I	355 × 355 mm (14 × 14 in)	2130 mm (84 in)	6	8T25 ($\rho_g = 3.2\%$)	T10–350 mm ($\rho_v = 0.12\%$)
J	355 × 355 mm (14 × 14 in)	2130 mm (84 in)	6	8T25 ($\rho_g = 3.2\%$)	T10–88 mm ($\rho_v = 0.46\%$)
K	355 × 355 mm (14 × 14 in)	2130 mm (84 in)	6	8T20 ($\rho_g = 1.8\%$)	T10–350 mm ($\rho_v = 0.12\%$)
L	355 × 355 mm (14 × 14 in)	2130 mm (84 in)	6	8T20 ($\rho_g = 1.8\%$)	T10–88 mm ($\rho_v = 0.46\%$)

Table 1

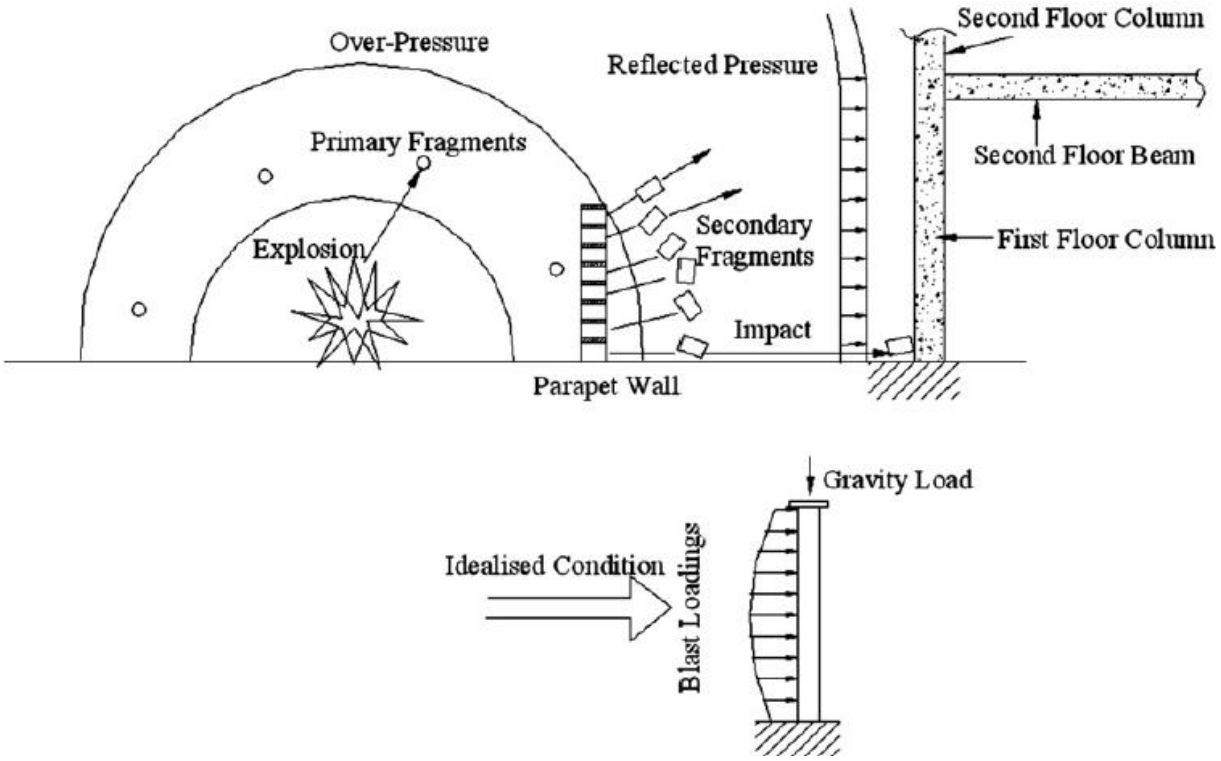
Over-Pressure
Reflected Pressure
Second Floor Column
Primary Fragments
Second Floor Beam
Explosion
Secondary Fragments
First Floor Column
Impact
Parapet Wall
Gravity Load
Idealised Condition
Blast Loadings

Fig. 1

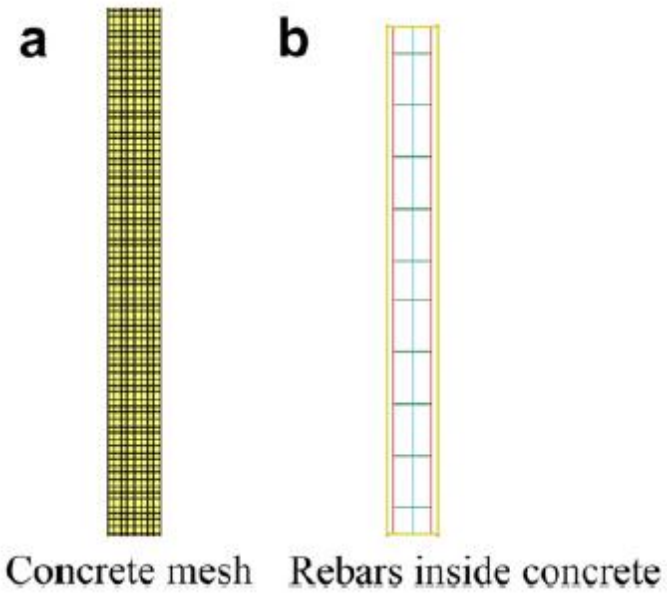

Fig. 2

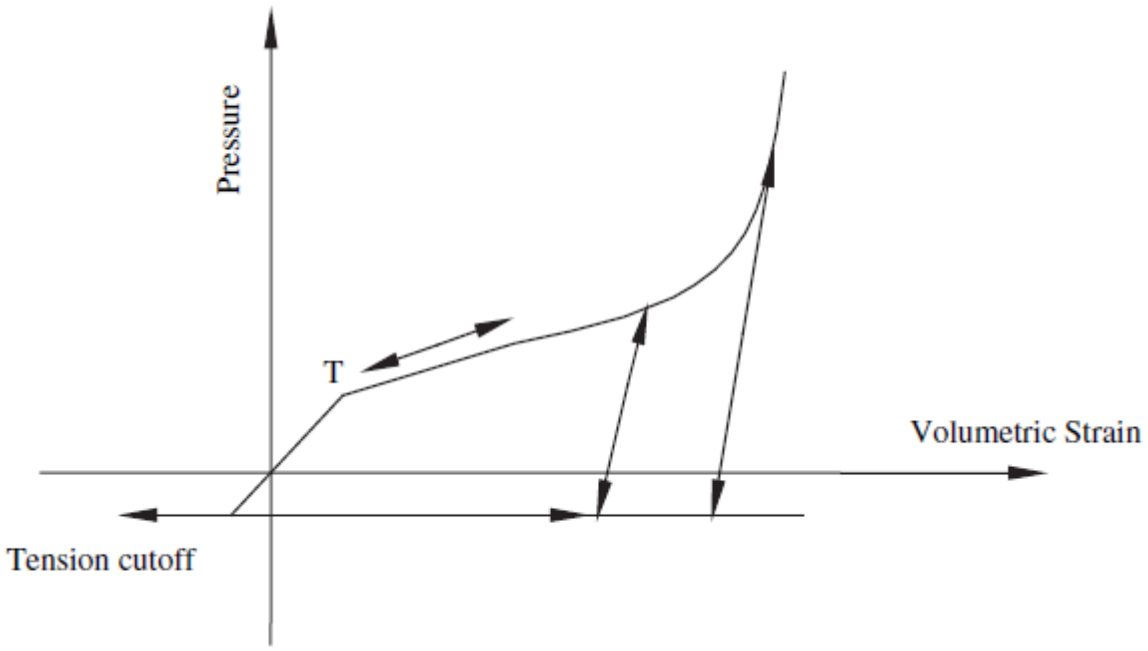

Fig. 3

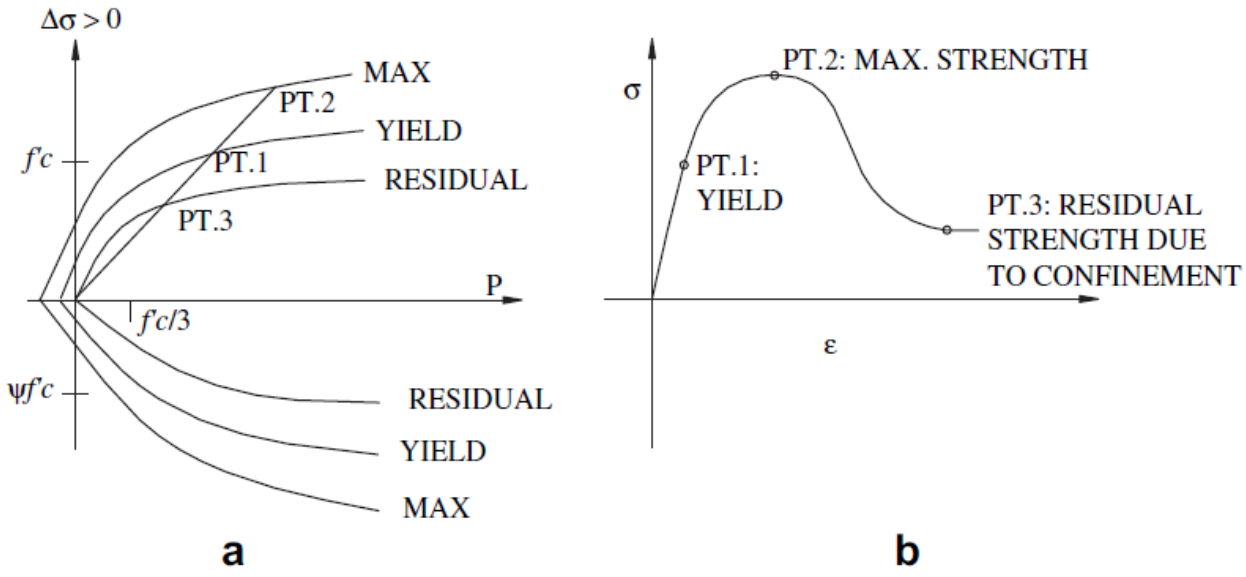
Δσ > 0
MAX
PT.2
YIELD
f'c
PT.1
RESIDUAL
PT.3
P
f'c/3
ψf'c
RESIDUAL
YIELD
MAX
a
σ
PT.2: MAX. STRENGTH
PT.1:
YIELD
PT.3: RESIDUAL
STRENGTH DUE
TO CONFINEMENT
ε
b

Fig. 4

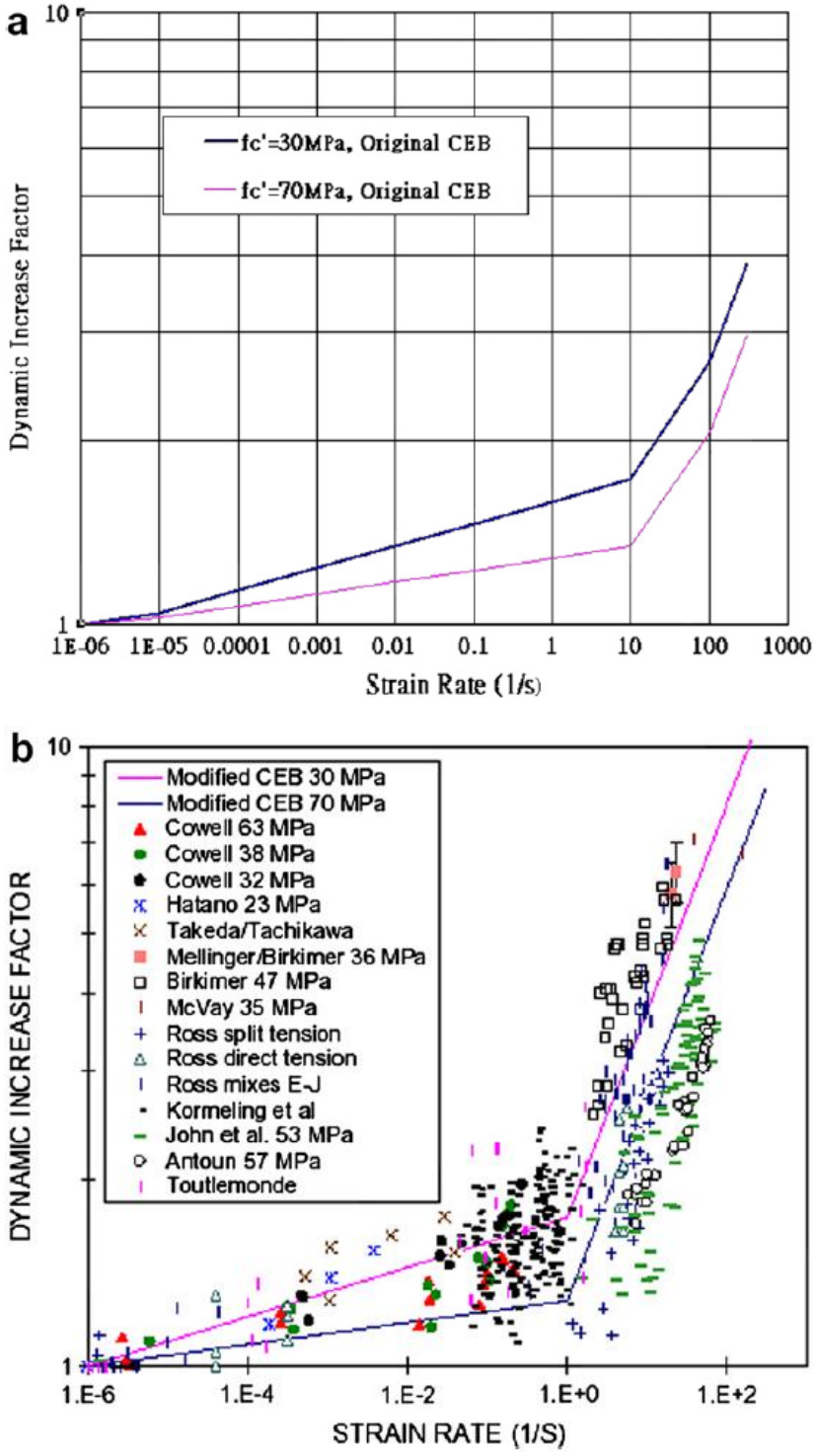
a
10
1
Dynamic Increase Factor
fc'=30MPa, Original CEB
fc'=70MPa, Original CEB
1E-06
1E-05
0.0001
0.001
0.01
0.1
1
10
100
1000
Strain Rate (1/s)
b
10
1
DYNAMIC INCREASE FACTOR
Modified CEB 30 MPa
Modified CEB 70 MPa
Cowell 63 MPa
Cowell 38 MPa
Cowell 32 MPa
Hatano 23 MPa
Takeda/Tachikawa
Mellinger/Birkimer 36 MPa
Birkimer 47 MPa
McVay 35 MPa
Ross split tension
Ross direct tension
Ross mixes E-J
Kormeling et al
John et al. 53 MPa
Antoun 57 MPa
Toutlemonde
1.E-6
1.E-4
1.E-2
1.E+0
1.E+2
STRAIN RATE (1/S)

Fig. 5

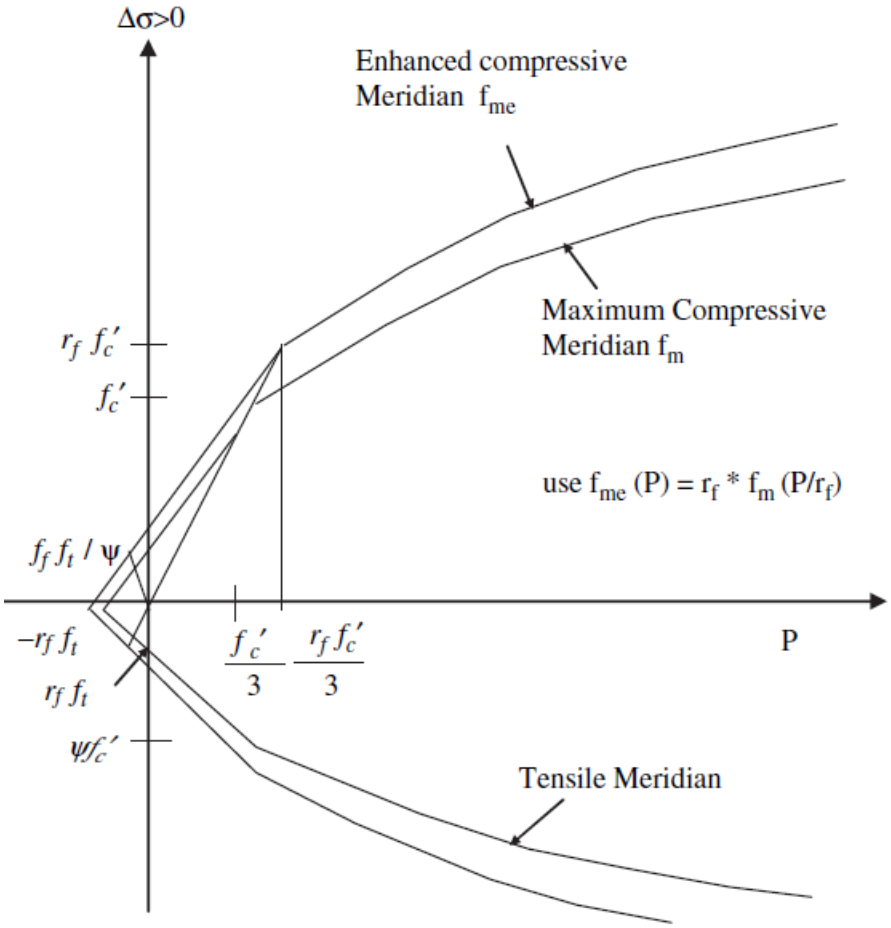
Δσ>0
Enhanced compressive
Meridian f_{me}
Maximum Compressive
Meridian f_m
use $f_{me}(P) = r_f * f_m(P/r_f)$
$r_f f_c'$
f_c'
$f_f f_t / \psi$
$-r_f f_t$
$r_f f_t$
$\psi f_c'$
$\frac{f_c'}{3}$
$\frac{r_f f_c'}{3}$
P
Tensile Meridian

Fig. 6

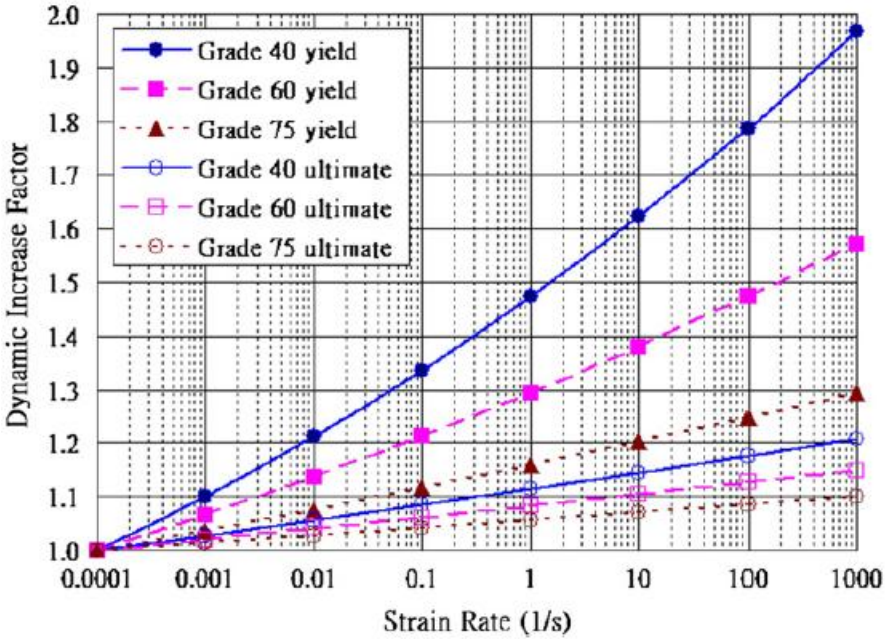
Grade 40 yield
Grade 60 yield
Grade 75 yield
Grade 40 ultimate
Grade 60 ultimate
Grade 75 ultimate
Dynamic Increase Factor
2.0
1.9
1.8
1.7
1.6
1.5
1.4
1.3
1.2
1.1
1.0
0.0001
0.001
0.01
0.1
1
10
100
1000
Strain Rate (1/s)

Fig. 7

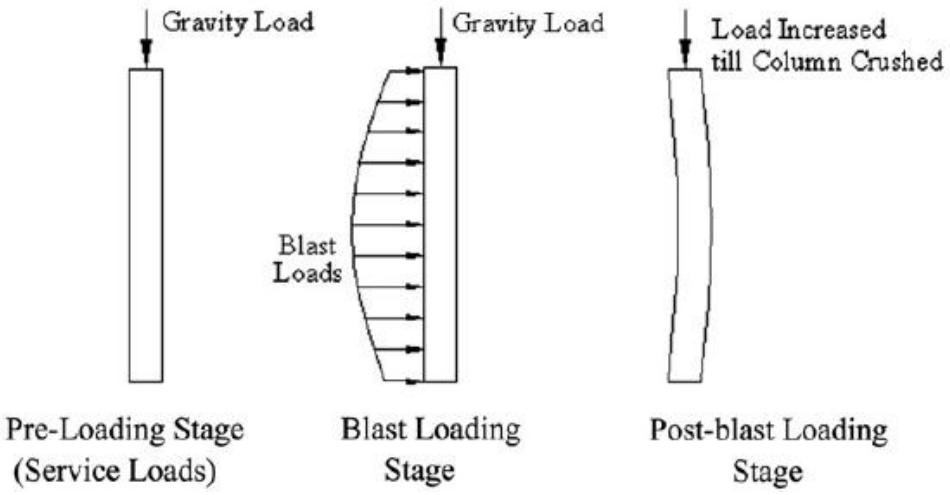
Gravity Load
Gravity Load
Load Increased
till Column Crushed
Blast
Loads
Pre-Loading Stage
(Service Loads)
Blast Loading
Stage
Post-blast Loading
Stage

Fig. 8

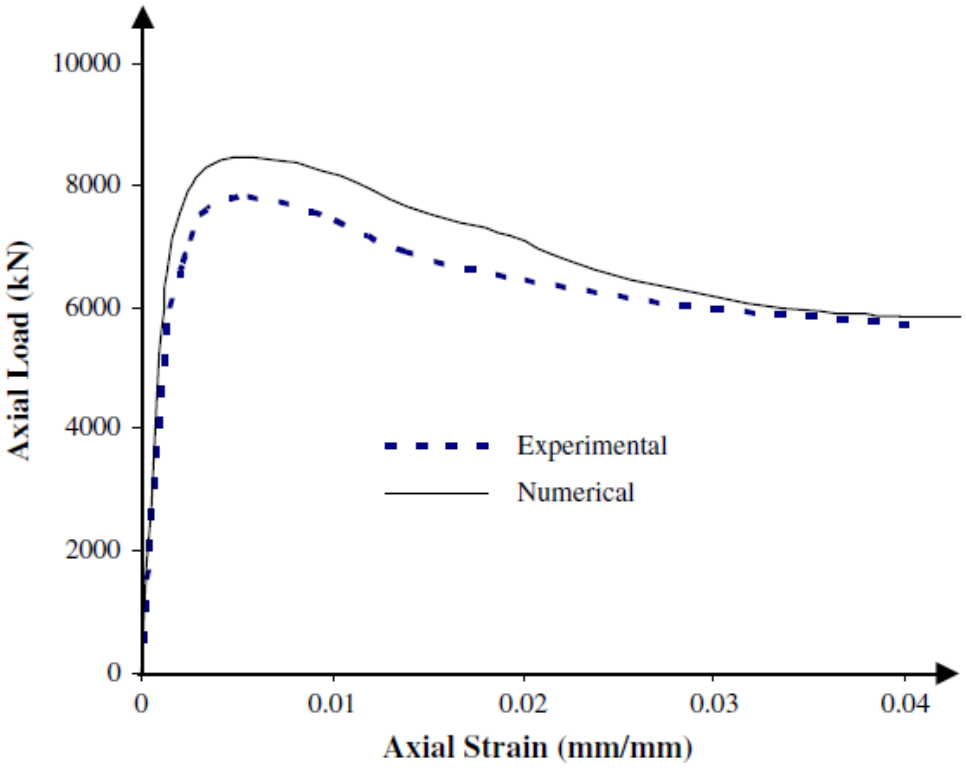
10000
8000
6000
4000
2000
0
Axial Load (kN)
0
0.01
0.02
0.03
0.04
Axial Strain (mm/mm)
Experimental
Numerical

Fig. 9

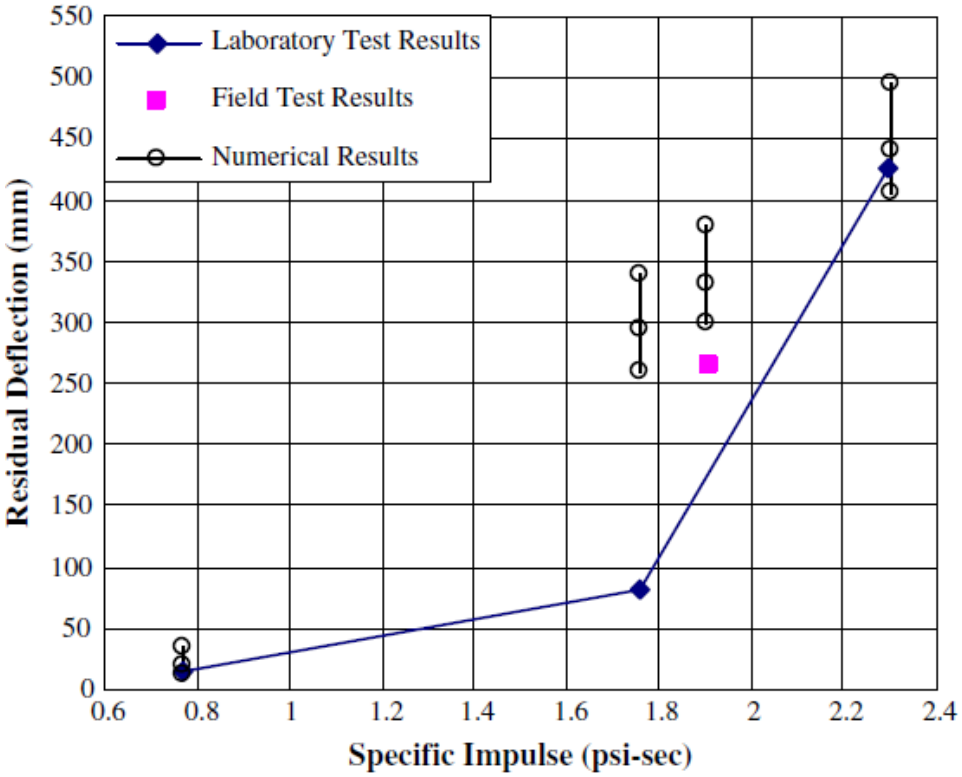
Laboratory Test Results
Field Test Results
Numerical Results
Residual Deflection (mm)
550
500
450
400
350
300
250
200
150
100
50
0
0.6
0.8
1
1.2
1.4
1.6
1.8
2
2.2
2.4
Specific Impulse (psi-sec)

Fig. 10

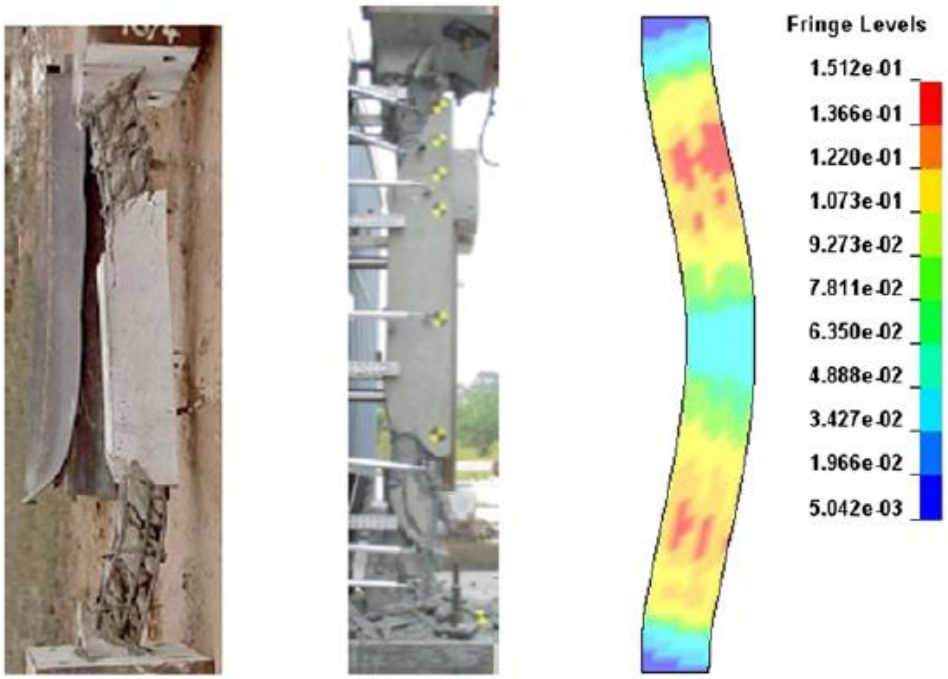

Field Test Blast Simulator Test Predicted Damage

Fig. 11

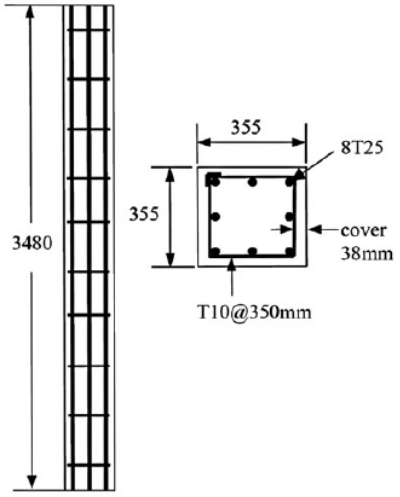

Series A Column

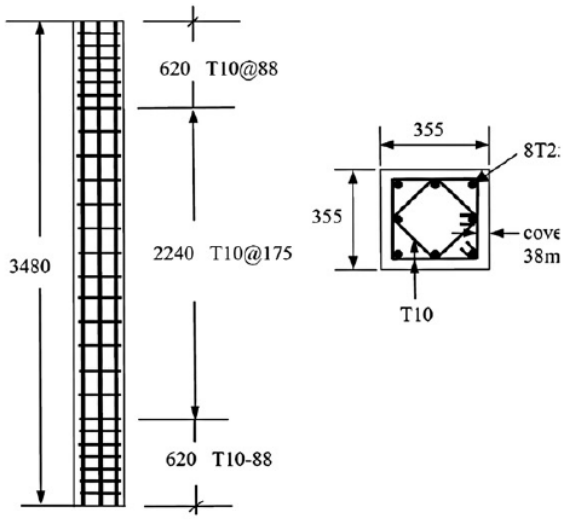

Series B Column

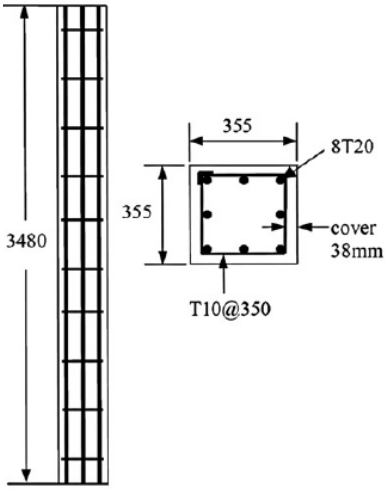

Series C Column

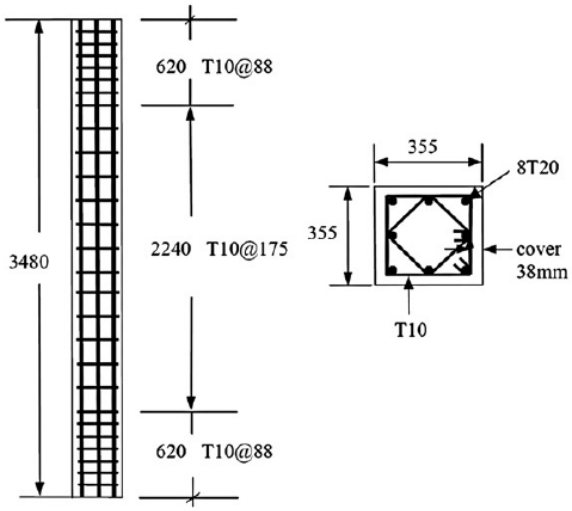

Series D Column

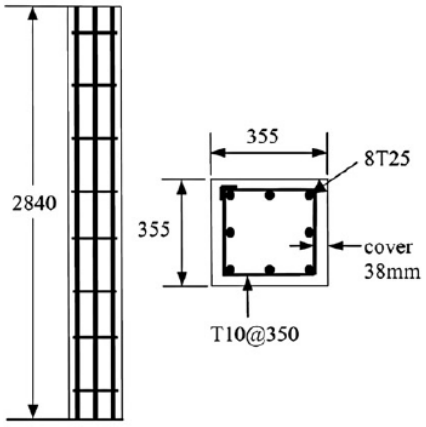

Series E Column

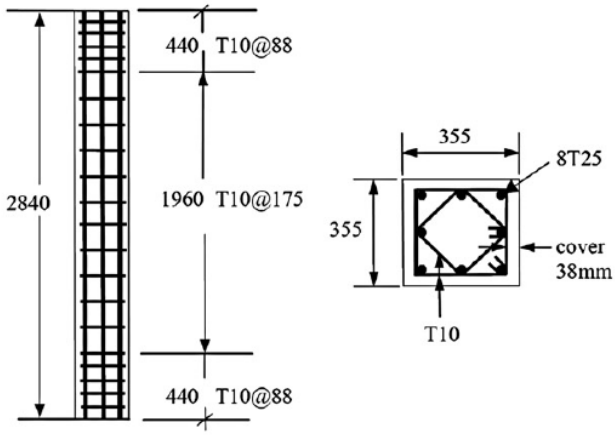

Series F Column

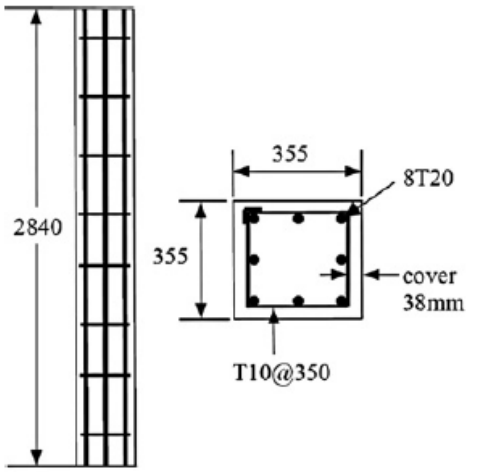

Series G Column

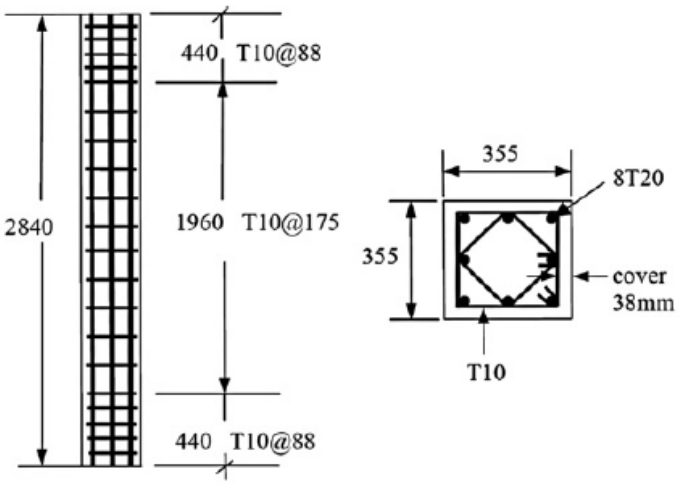

Series H Column

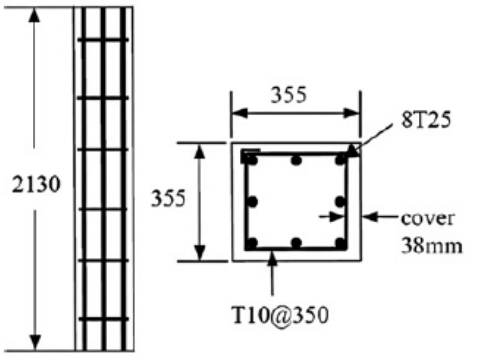

Series I Column

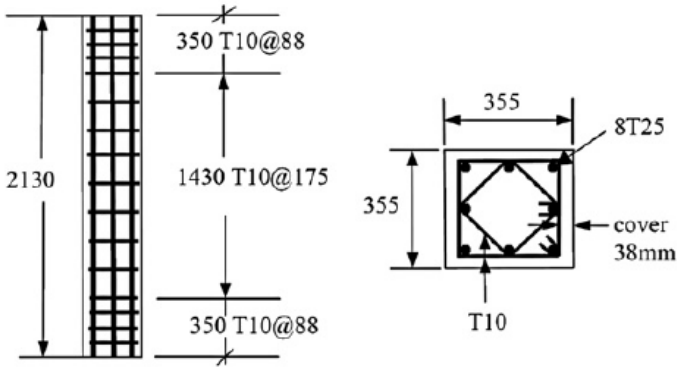

Series J Column

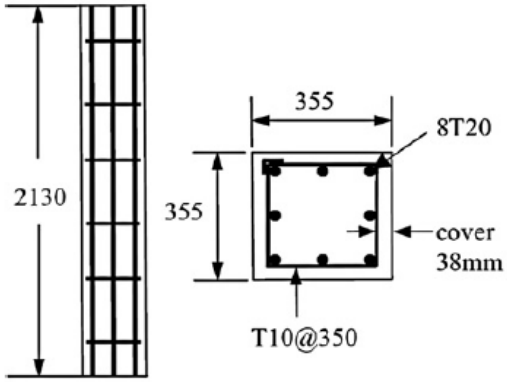

Series K Column

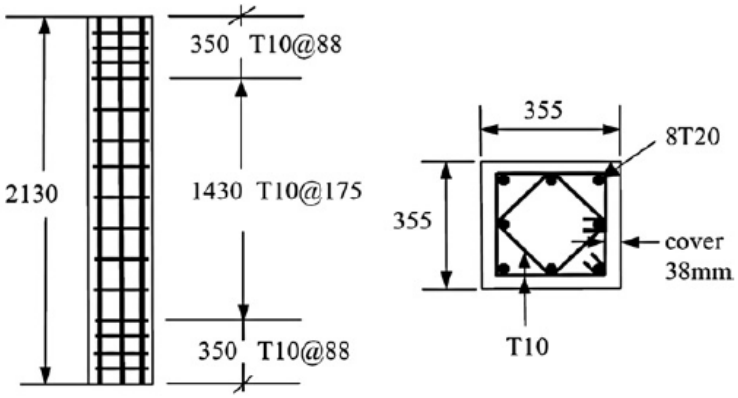

Series L Column

Fig. 12

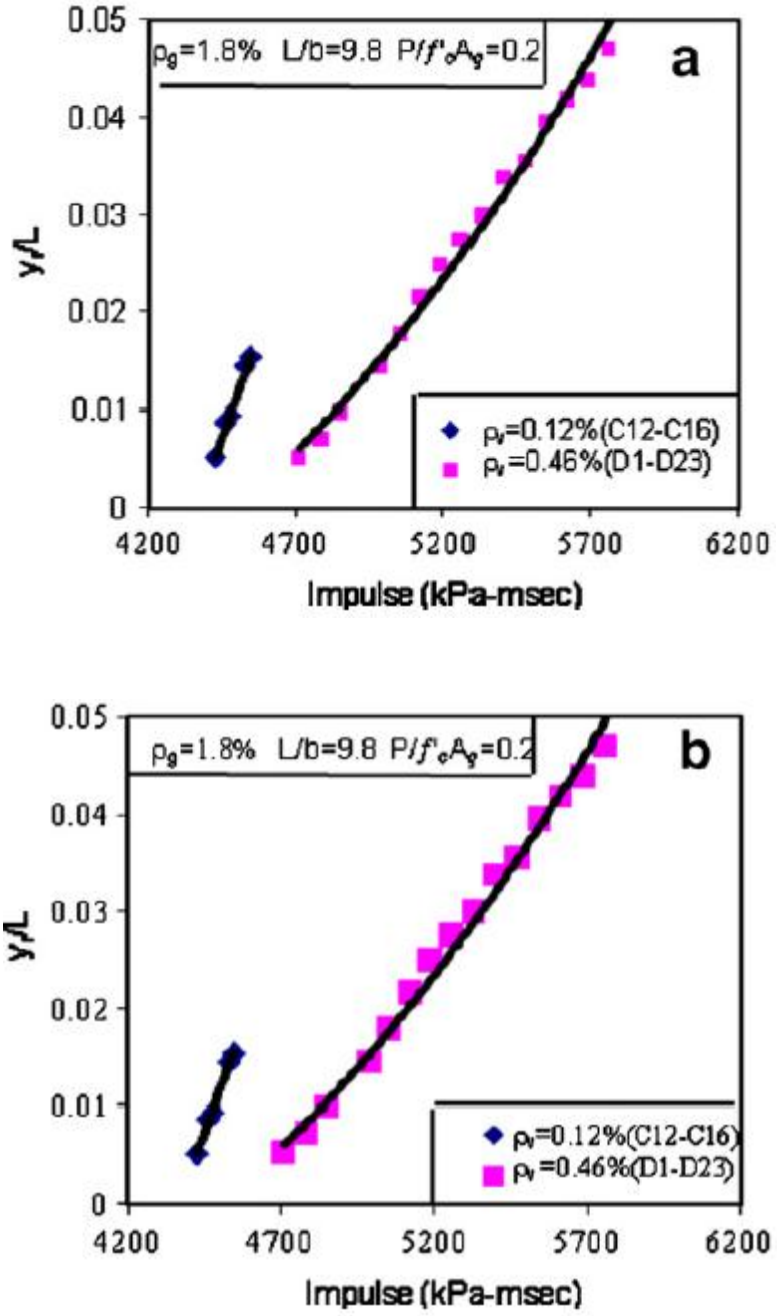
0.05
0.04
0.03
0.02
0.01
0
y/L
ρg=1.8% L/b=9.8 P/f'cAg=0.2
a
ρv=0.12%(C12-C16)
ρv=0.46%(D1-D23)
4200
4700
5200
5700
6200
Impulse (kPa-msec)
0.05
0.04
0.03
0.02
0.01
0
y/L
ρg=1.8% L/b=9.8 P/f'cAg=0.2
b
ρv=0.12%(C12-C16)
ρv=0.46%(D1-D23)
4200
4700
5200
5700
6200
Impulse (kPa-msec)

Fig. 13

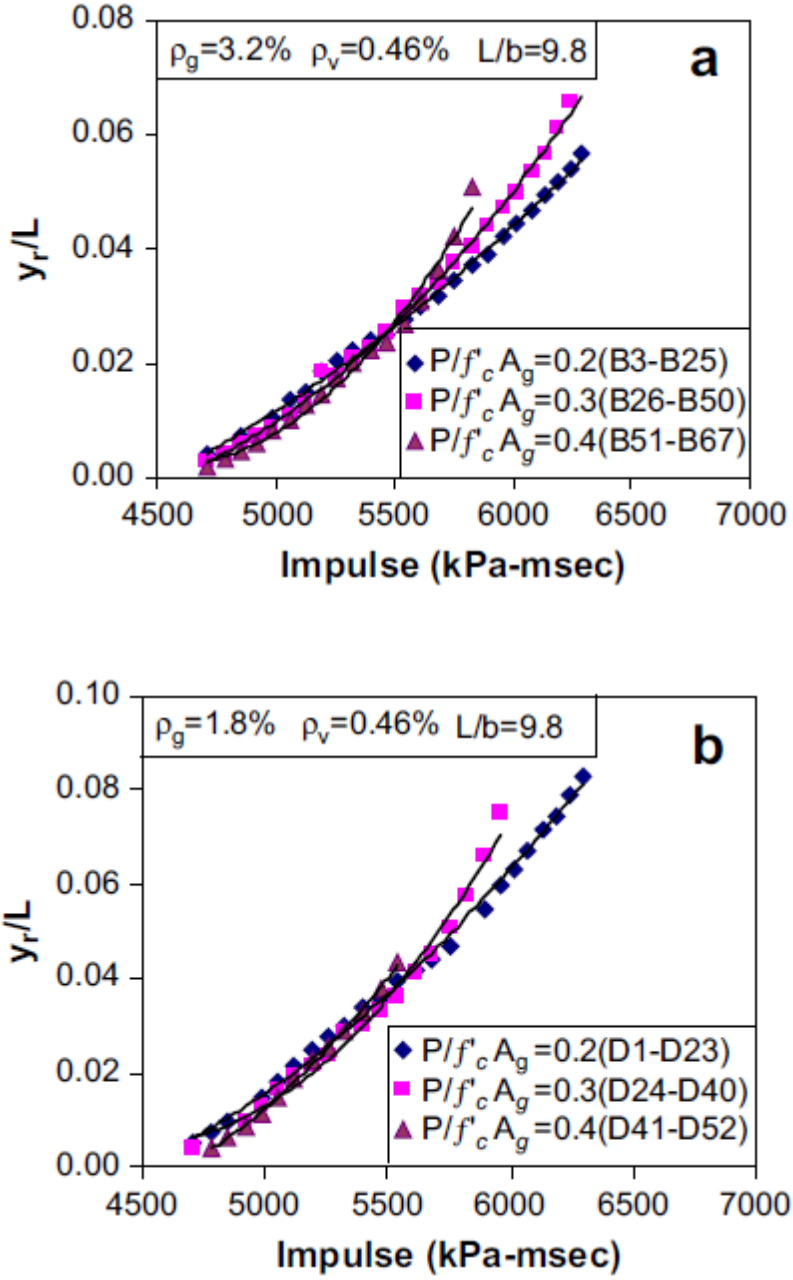
a
ρg=3.2% ρv=0.46% L/b=9.8
P/f'c Ag=0.2(B3-B25)
P/f'c Ag=0.3(B26-B50)
P/f'c Ag=0.4(B51-B67)
yr/L
Impulse (kPa-msec)
0.00
0.02
0.04
0.06
0.08
4500
5000
5500
6000
6500
7000
b
ρg=1.8% ρv=0.46% L/b=9.8
P/f'c Ag=0.2(D1-D23)
P/f'c Ag=0.3(D24-D40)
P/f'c Ag=0.4(D41-D52)
yr/L
Impulse (kPa-msec)
0.00
0.02
0.04
0.06
0.08
0.10
4500
5000
5500
6000
6500
7000

Fig. 14

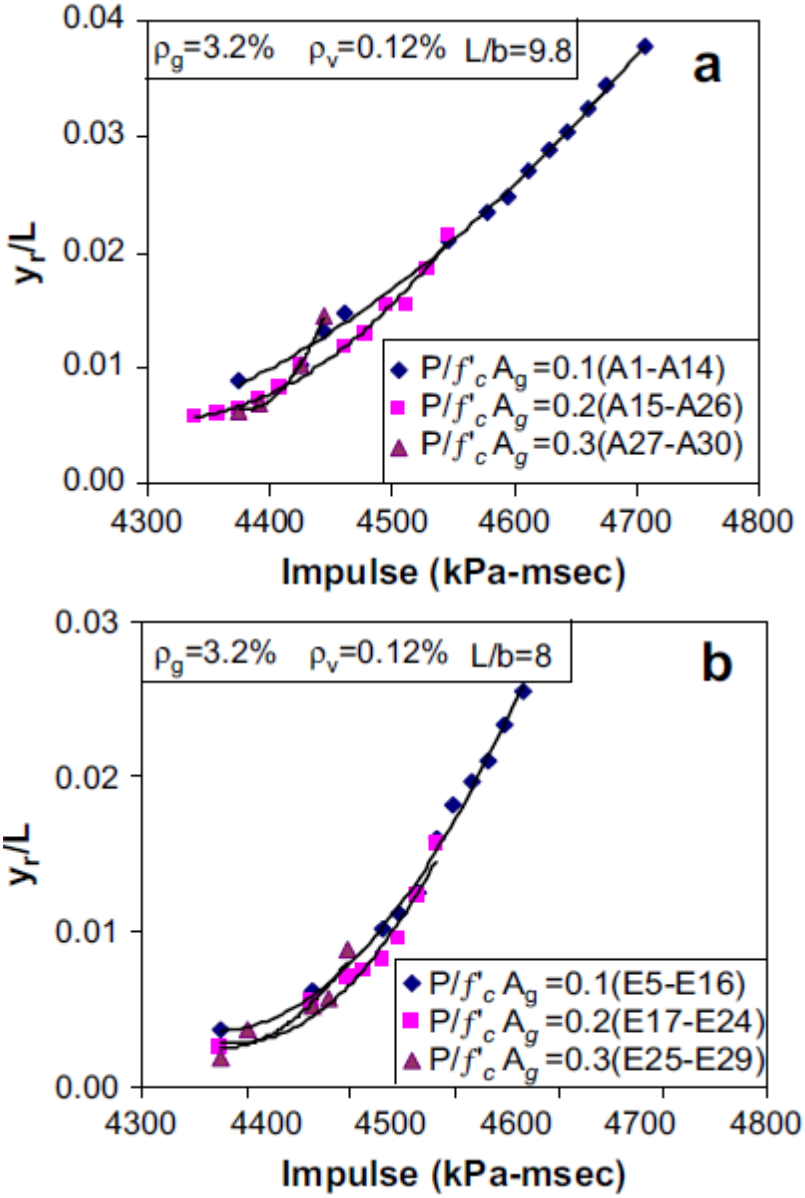
0.04
0.03
0.02
0.01
0.00
y_r/L
ρ_g=3.2% ρ_v=0.12% L/b=9.8
a
P/f'_c A_g =0.1(A1-A14)
P/f'_c A_g =0.2(A15-A26)
P/f'_c A_g =0.3(A27-A30)
4300
4400
4500
4600
4700
4800
Impulse (kPa-msec)
0.03
0.02
0.01
0.00
y_r/L
ρ_g=3.2% ρ_v=0.12% L/b=8
b
P/f'_c A_g =0.1(E5-E16)
P/f'_c A_g =0.2(E17-E24)
P/f'_c A_g =0.3(E25-E29)
4300
4400
4500
4600
4700
4800
Impulse (kPa-msec)

Fig. 15

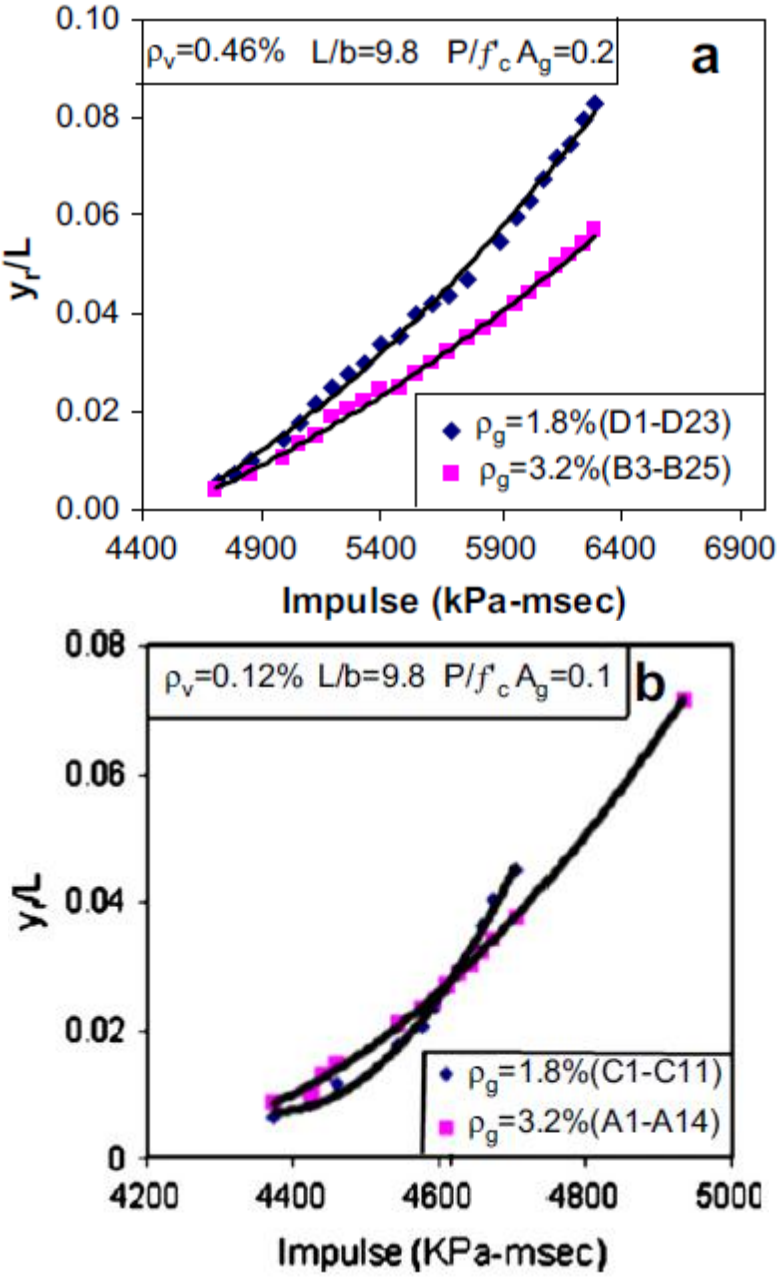
a
ρ_v=0.46% L/b=9.8 P/$f'_c A_g$=0.2
ρ_g=1.8%(D1-D23)
ρ_g=3.2%(B3-B25)
y_r/L
0.10
0.08
0.06
0.04
0.02
0.00
4400
4900
5400
5900
6400
6900
Impulse (kPa-msec)
b
ρ_v=0.12% L/b=9.8 P/$f'_c A_g$=0.1
ρ_g=1.8%(C1-C11)
ρ_g=3.2%(A1-A14)
y/L
0.08
0.06
0.04
0.02
0
4200
4400
4600
4800
5000
Impulse (KPa-msec)

Fig. 16

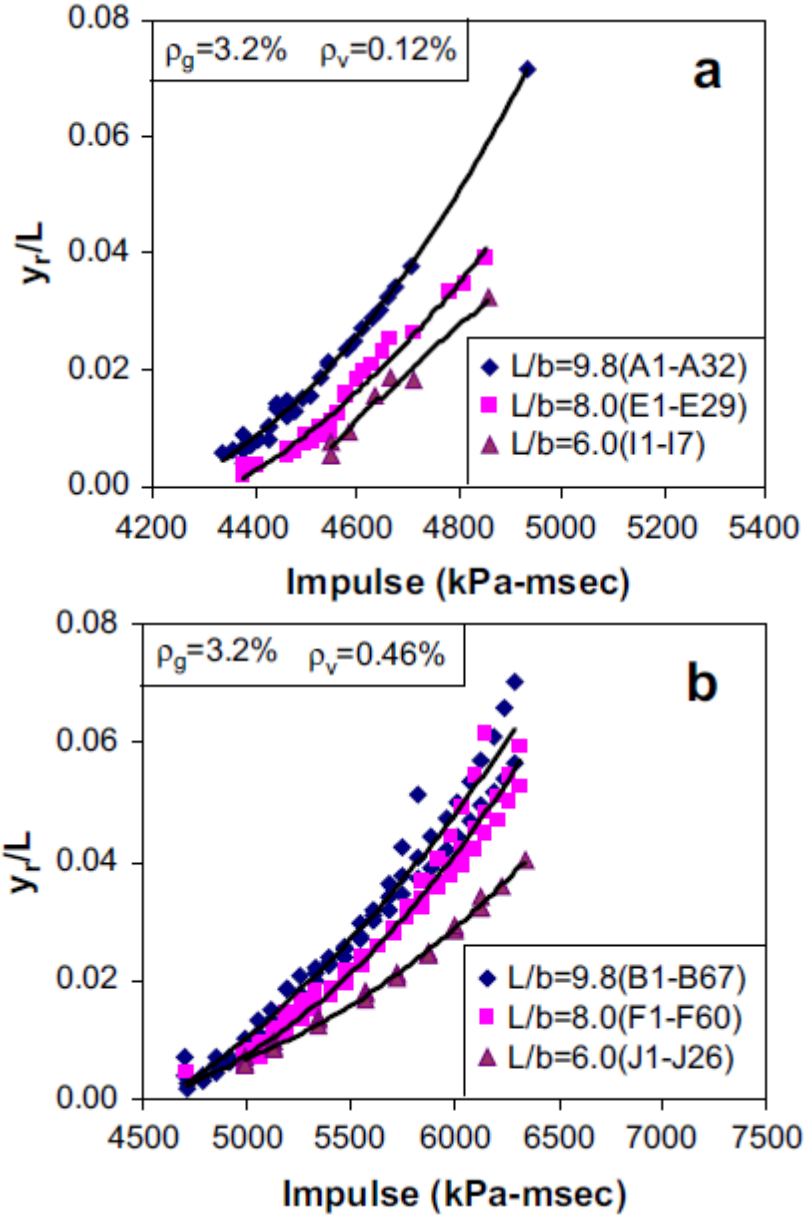
0.08
0.06
0.04
0.02
0.00
y_r/L
ρ_g=3.2% ρ_v=0.12%
a
L/b=9.8(A1-A32)
L/b=8.0(E1-E29)
L/b=6.0(I1-I7)
4200 4400 4600 4800 5000 5200 5400
Impulse (kPa-msec)
0.08
0.06
0.04
0.02
0.00
y_r/L
ρ_g=3.2% ρ_v=0.46%
b
L/b=9.8(B1-B67)
L/b=8.0(F1-F60)
L/b=6.0(J1-J26)
4500 5000 5500 6000 6500 7000 7500
Impulse (kPa-msec)

Fig. 17

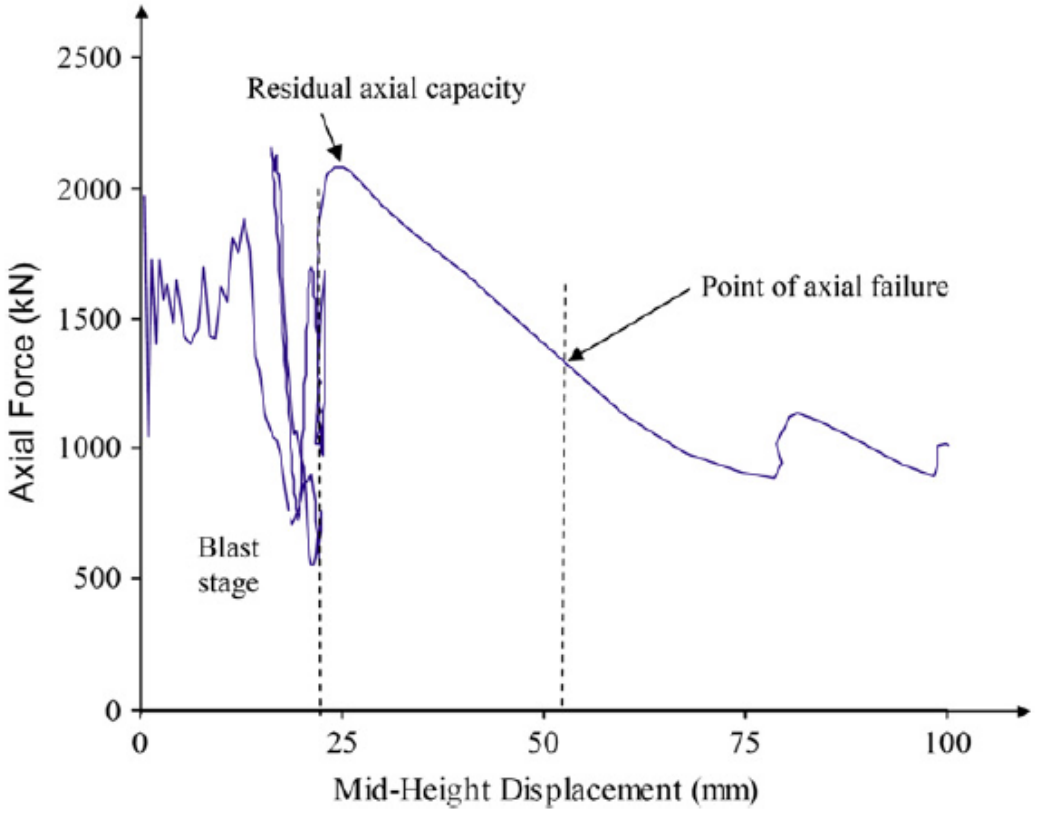
2500
2000
1500
1000
500
0
Axial Force (kN)
Residual axial capacity
Point of axial failure
Blast
stage
0
25
50
75
100
Mid-Height Displacement (mm)

Fig. 18

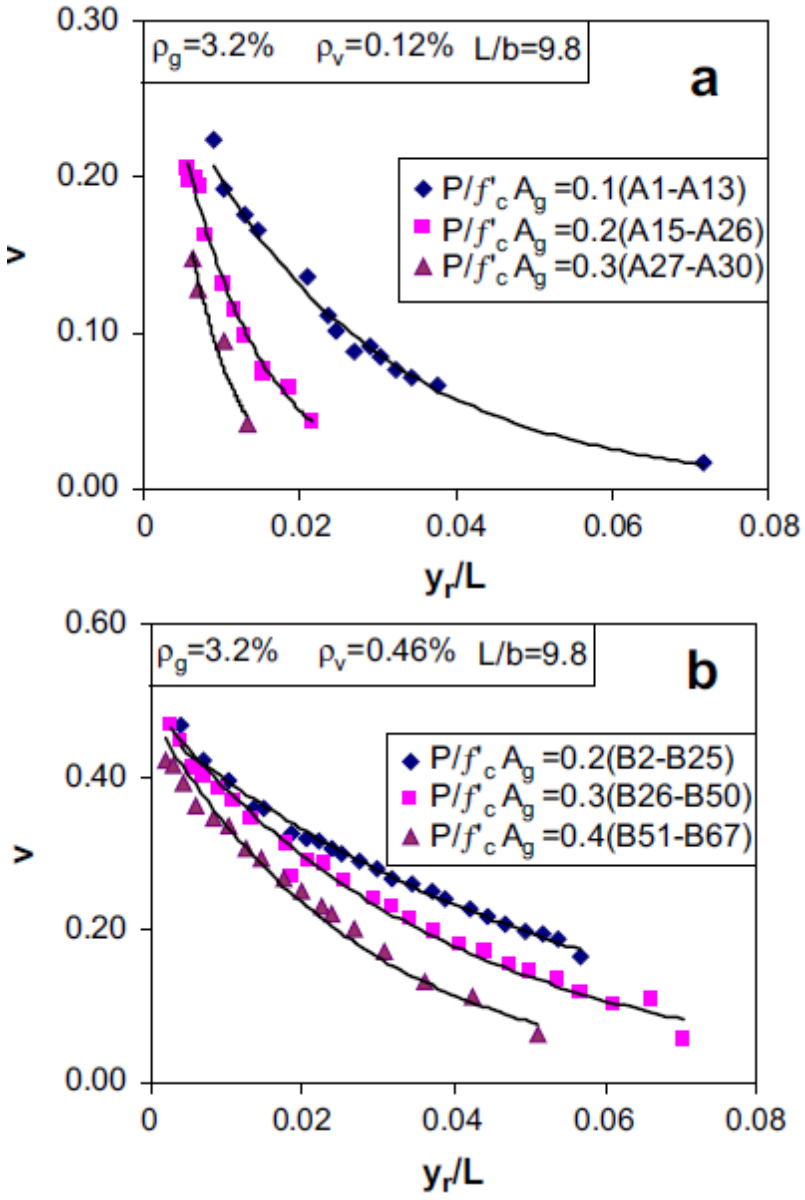
ρg=3.2% ρv=0.12% L/b=9.8
a
P/f'c Ag =0.1(A1-A13)
P/f'c Ag =0.2(A15-A26)
P/f'c Ag =0.3(A27-A30)
v
yr/L
0.30
0.20
0.10
0.00
0
0.02
0.04
0.06
0.08
ρg=3.2% ρv=0.46% L/b=9.8
b
P/f'c Ag =0.2(B2-B25)
P/f'c Ag =0.3(B26-B50)
P/f'c Ag =0.4(B51-B67)
v
yr/L
0.60
0.40
0.20
0.00
0
0.02
0.04
0.06
0.08

Fig. 19

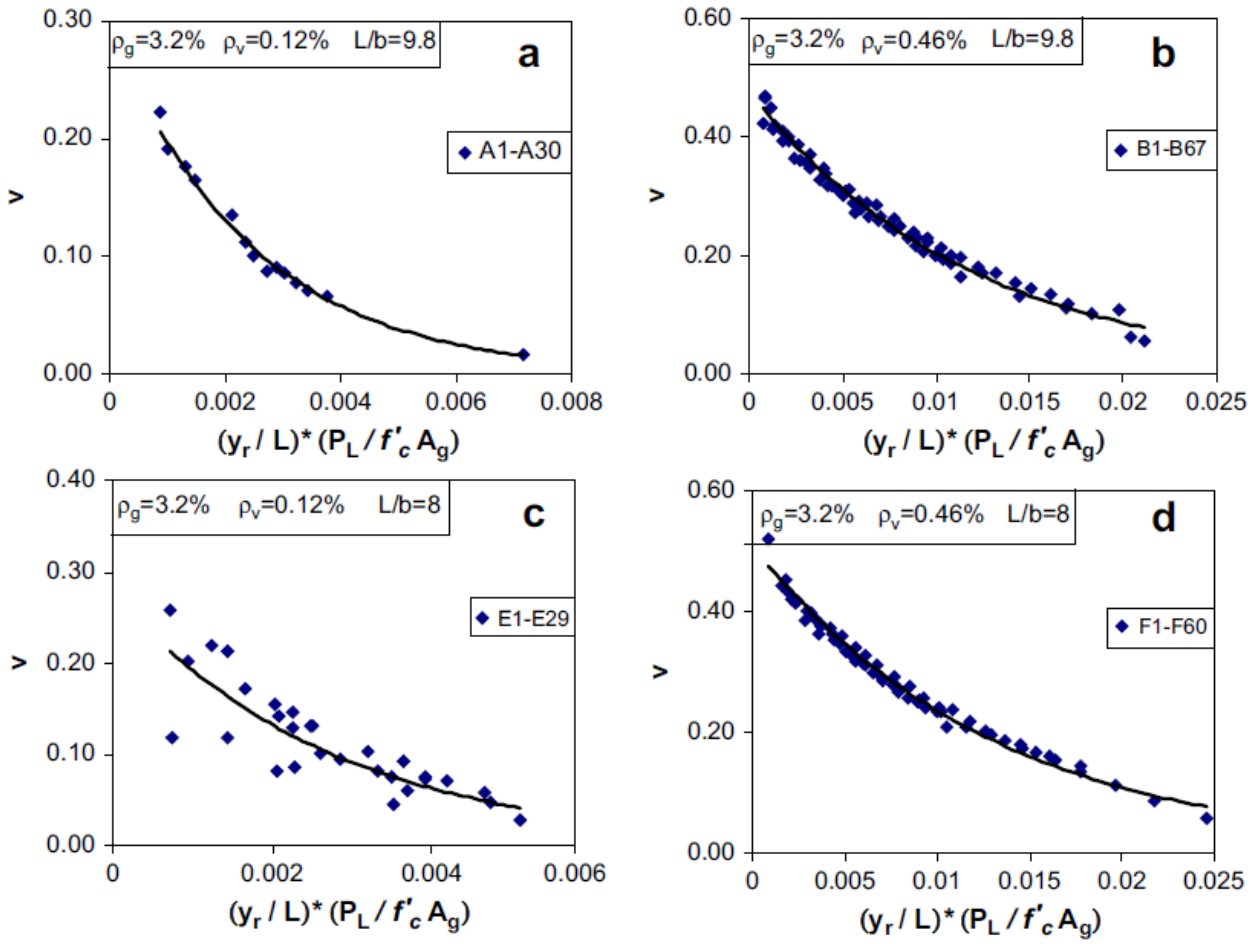
ρg=3.2% ρv=0.12% L/b=9.8
a
A1-A30
v
(yr / L)* (PL / f'c Ag)
ρg=3.2% ρv=0.46% L/b=9.8
b
B1-B67
ρg=3.2% ρv=0.12% L/b=8
c
E1-E29
ρg=3.2% ρv=0.46% L/b=8
d
F1-F60

Fig. 20

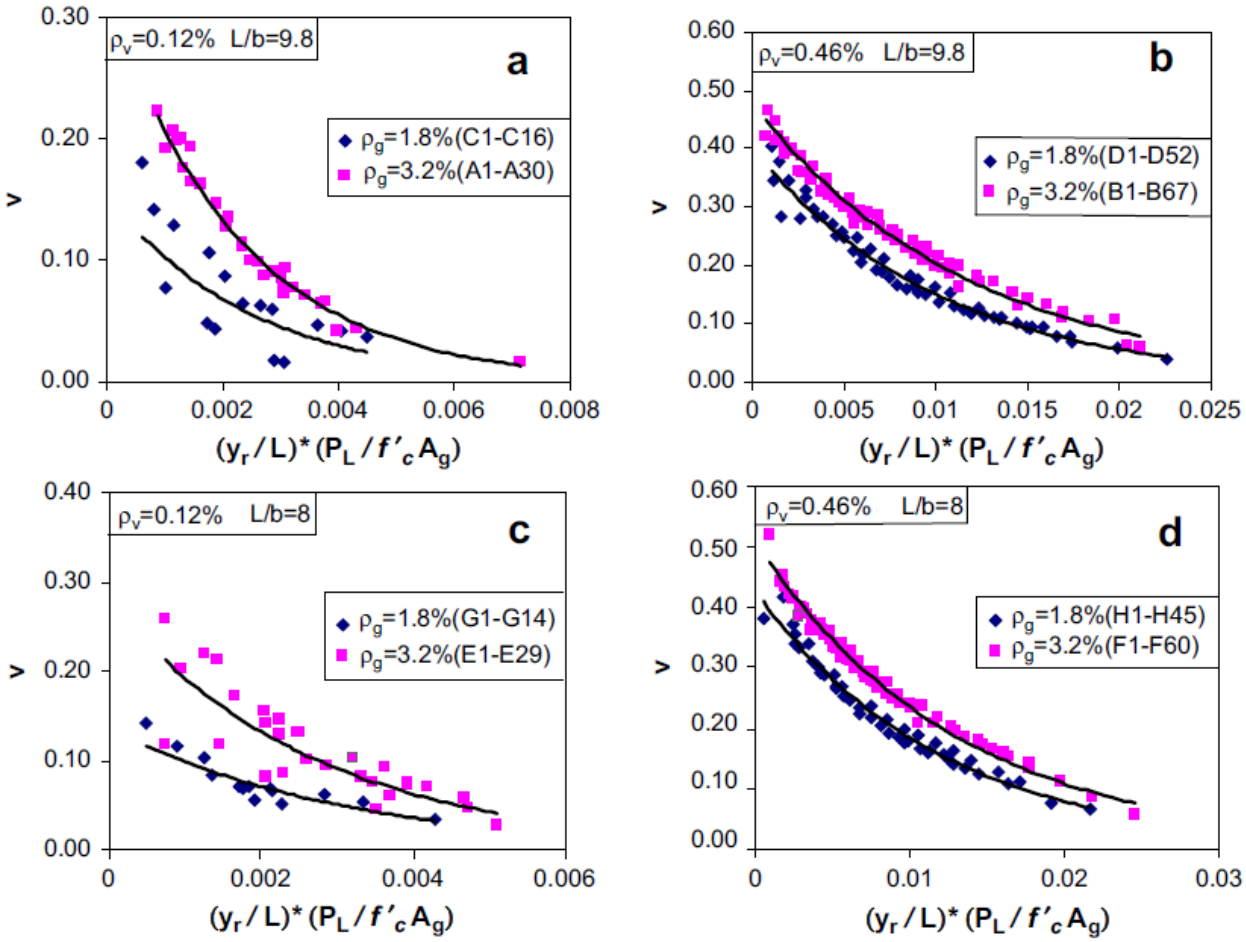
a
ρv=0.12% L/b=9.8
ρg=1.8%(C1-C16)
ρg=3.2%(A1-A30)
v
(yr / L)* (PL / f′c Ag)
b
ρv=0.46% L/b=9.8
ρg=1.8%(D1-D52)
ρg=3.2%(B1-B67)
c
ρv=0.12% L/b=8
ρg=1.8%(G1-G14)
ρg=3.2%(E1-E29)
d
ρv=0.46% L/b=8
ρg=1.8%(H1-H45)
ρg=3.2%(F1-F60)

Fig. 21

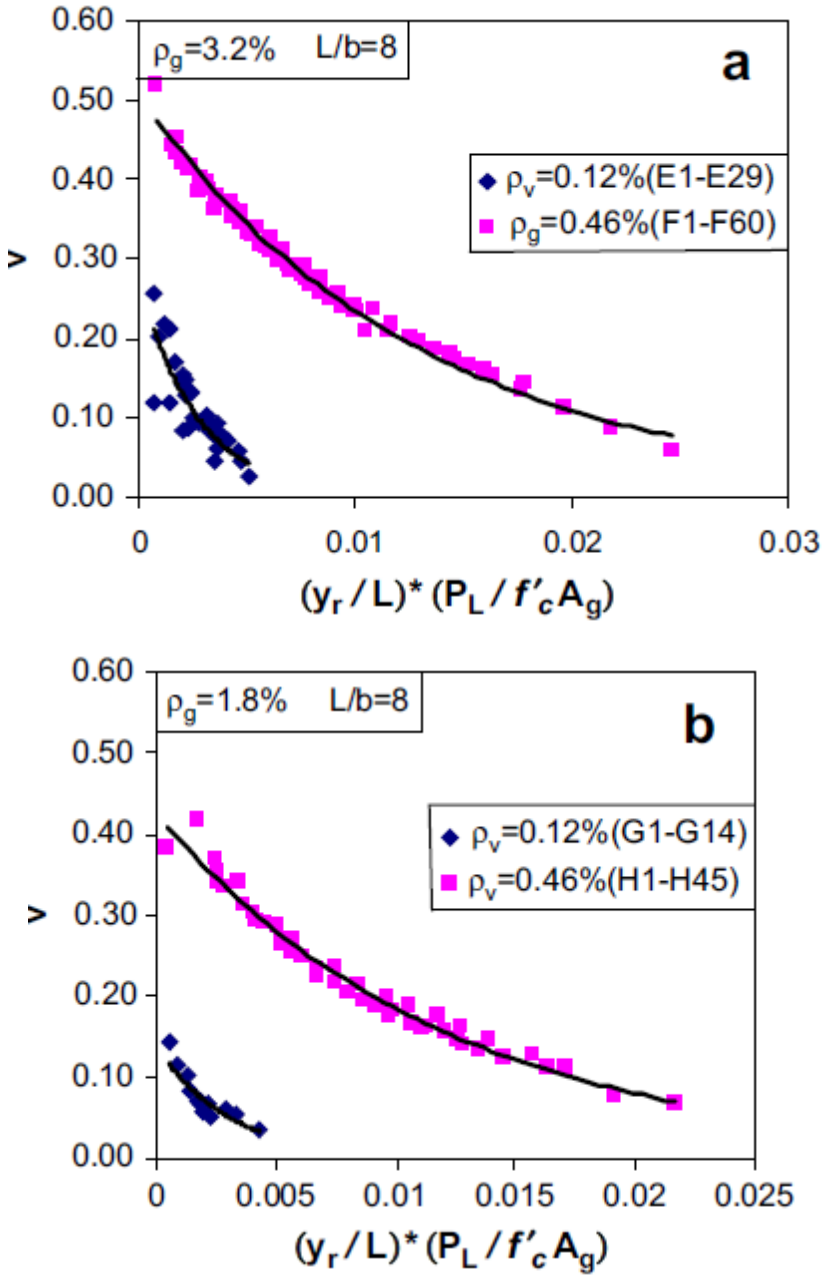
a
ρg=3.2% L/b=8
ρv=0.12%(E1-E29)
ρg=0.46%(F1-F60)
v
0.60
0.50
0.40
0.30
0.20
0.10
0.00
0
0.01
0.02
0.03
(yr / L)* (PL / f′c Ag)
b
ρg=1.8% L/b=8
ρv=0.12%(G1-G14)
ρv=0.46%(H1-H45)
v
0.60
0.50
0.40
0.30
0.20
0.10
0.00
0
0.005
0.01
0.015
0.02
0.025
(yr / L)* (PL / f′c Ag)

Fig. 22

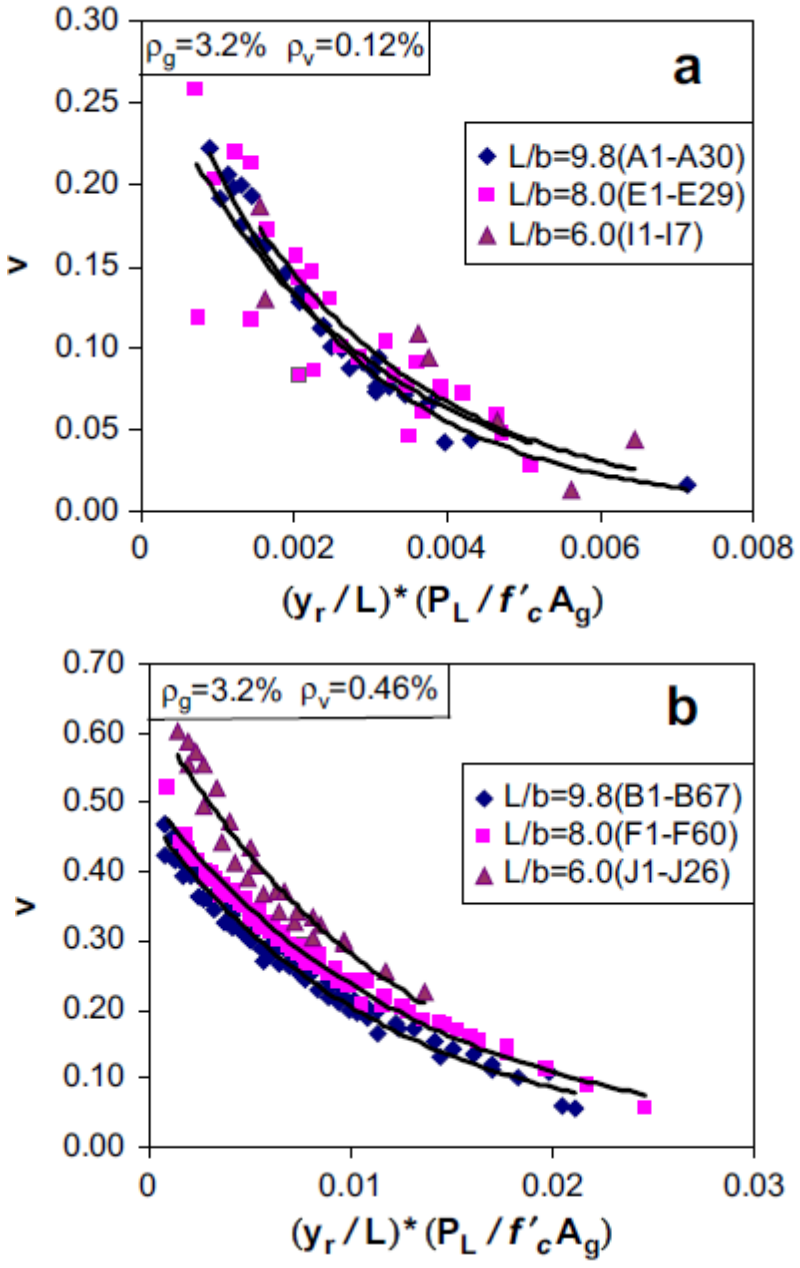
a
ρg=3.2% ρv=0.12%
L/b=9.8(A1-A30)
L/b=8.0(E1-E29)
L/b=6.0(I1-I7)
v
0.30
0.25
0.20
0.15
0.10
0.05
0.00
0
0.002
0.004
0.006
0.008
(yr / L)* (PL / f′c Ag)
b
ρg=3.2% ρv=0.46%
L/b=9.8(B1-B67)
L/b=8.0(F1-F60)
L/b=6.0(J1-J26)
v
0.70
0.60
0.50
0.40
0.30
0.20
0.10
0.00
0
0.01
0.02
0.03
(yr / L)* (PL / f′c Ag)

Fig. 23

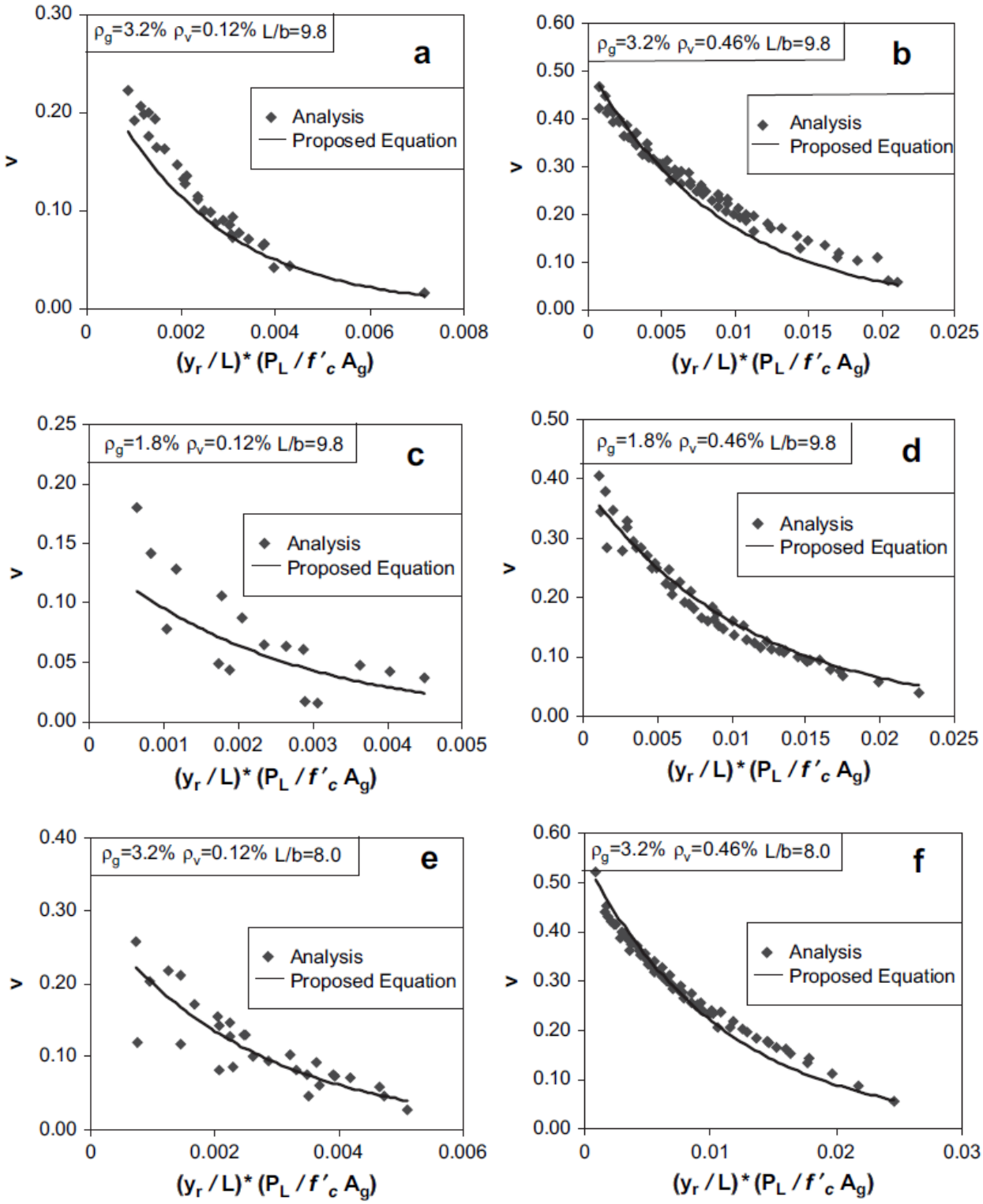
ρg=3.2% ρv=0.12% L/b=9.8
a
Analysis
Proposed Equation
v
(yr / L)* (PL / f′c Ag)
ρg=3.2% ρv=0.46% L/b=9.8
b
ρg=1.8% ρv=0.12% L/b=9.8
c
ρg=1.8% ρv=0.46% L/b=9.8
d
ρg=3.2% ρv=0.12% L/b=8.0
e
ρg=3.2% ρv=0.46% L/b=8.0
f

Fig. 24